The cation channel mechanisms of subthreshold inward depolarizing currents in the VTA dopaminergic neurons and their roles in the chronic-stress-induced depression-like behavior

Jing Wang[1,3], Min Su[1,4], Dongmei Zhang[1,5], Ludi Zhang[1], Chenxu Niu[1], Chaoyi Li[1], Shuangzhu You[1], Yuqi Sang[1,6,7], Yongxue Zhang[1,8], Xiaona Du[1], Hailin Zhang[1,2*]

[1]Department of Pharmacology; The Key Laboratory of Neural and Vascular Biology, Ministry of Education; The Key Laboratory of New Drug Pharmacology and Toxicology, Hebei Medical University, Shijiazhuang, Hebei, China
[2]Department of Psychiatry, The First Hospital of Hebei Medical University, Mental Health Institute of Hebei Medical University, China
[3]Department of Pharmacochemistry, Hebei University of Chinese Medicine, Shijiazhuang, Hebei, China
[4]Yiling Pharmaceutical Company, Shijiazhuang, Hebei, China
[5]Department of Clinical Pharmacy, Xintai Ninth Hoapital, Xintai, Hebei, China
[6]College of Chemical Engineering, Shijiazhuang University, Shijiazhuang, Hebei, China
[7] Shijiazhuang Key Laboratory of Targeted Drugs Research and Efficacy Evaluation, Shijiazhuang, Hebei, China
[8]Department of Pharmacy, Handan First Hospital, Handan, Hebei, China

*** Correspondence:**
Hailin Zhang
zhanghl@hebmu.edu.cn

Abstract:

The slow-intrinsic-pacemaker dopaminergic (DA) neurons originating in the ventral tegmental area (VTA) are implicated in various mood- and emotion-related disorders, such as anxiety, fear, stress and depression. Abnormal activity of projection-specific VTA DA neurons is the key factor in the development of these disorders. Here, we describe the crucial role for the NALCN and TRPC6, non-selective cation channels in mediating the subthreshold inward depolarizing current and driving the firing of action potentials of VTA DA neurons in physiological condition. Furthermore, we demonstrate that down-regulation of TRPC6 protein expression in the VTA DA neurons likely contributes to the reduced activity of projection-specific VTA DA

neuron in chronic mild unpredictable stress (CMUS) depressive mice. In consistent with these, selective knockdown of TRPC6 channels in the VTA DA neurons conferred mice with depression-like behavior. This current study suggests down-regulation of TRPC6 expression/function is involved in reduced VTA DA neuron firing and chronic stress-induced depression-like behavior of mice.

Keywords: Ventral tegmental area, Dopaminergic neurons, Cation channels, NALCN, TRPC6 channel

Introduction

Dopaminergic (DA) neurons in the ventral tegmental area (VTA) play a key role in mood, reward and emotion-related behaviors[1]. These DA neurons project, through mesocorticolimbic dopaminergic system, to brain regions including the nucleus accumbens (NAc), medial prefrontal cortex (mPFC) and basolateral amygdala (BLA), and modulate these target neuronal circuits through their regulated activity (firing of action potentials)[2, 3]. As such, understandably, the altered functional activity of the VTA DA neurons is found to be the key determinants in abnormal behaviors related to the diseased conditions such as depression- or anxiety-related states[4]. Thus, the study on the mechanism underlying the firing activity of the VTA DA neurons is crucial for understanding the function of the DA circuitry and the pathogenesis of related mental diseases[4-8].

The VTA DA neurons are slow intrinsic pacemakers, which are further modulated by synaptic inputs from multiple excitatory and inhibitory projections[9, 10]. Firing activity controls the release of DA, thus function of the VTA DA neurons. The altered activity of the VTA DA neurons in a pathological state includes altered firing frequency and switch of the firing patterns[7, 11].

The research on the mechanism for spontaneous firing of action potential (AP) is the key to understand functional regulation of the VTA DA neurons. A variety of ion channels (e.g. voltage-gated Na^+ channels, high-threshold-activated Ca^{2+} channels, Kv2, large conductance calcium-activated potassium channels, A- and M-type potassium channels) are reported to be involved in regulation of the spontaneous firing activity of midbrain DA neurons (including the substantia nigra pars compacta,

SNc and VTA)[12-22]. However, it is not completely clear how this spontaneous firing is initiated. AP fires when the resting membrane potential (RMP) is depolarized to the activation threshold for the voltage-dependent Na^+ channels, which results in opening of Na^+ channels and the upstroke of AP[12]. Therefore, a controlled depolarization of the RMP to the activation threshold of AP is the first key step in a cascade leading to firing of AP. In the VTA DA neurons, the identity of ion channels contributing to this subthreshold depolarization has not been unambiguously established.

The hyperpolarization-activated cyclic-nucleotide-modulated (HCN1-4) channel gene family, one non-selective cation channels that would be activated at a hyperpolarized membrane potential[23], represent the molecular correlates of the pacemaker current in some cells with spontaneous firing of AP, such as If in cardiomyocytes and Ih in certain neurons including a subset of midbrain SNc DA neurons[23]. However, in the VTA DA neurons, results concerning the HCN channels to the spontaneous firing are controversial[15, 23-25].

Another non-selective cation channel, NALCN, unlike HCN, is a voltage-modulated channel[26], and is reported to be among the candidates for molecular correlates of the persistent background Na^+ leak currents in the VTA DA neurons [27, 28]. The NALCN-mediated background Na^+ leak currents are found to be involved in modulation of firing activity in a variety of neurons including DA neurons in the SNc[28-32]. However, it has not been reported if NALCN plays a role in spontaneous firing of the VTA DA neurons, although the VTA DA neurons have larger Na^+ leak currents than SNc DA neurons do[15].

TRP channels are a large class of non-selective cation channels, and are widely distributed in the peripheral and central nervous system. TRPC3, which has a high homology with TRPC6[33], is found to be involved in the regulation of cardiac and SNc DA neuronal excitability, generating depolarizing currents, triggering action potentials and participating in cellular rhythmic firing[32, 34, 35].The role of TRP channels, except TRPC4[36], in the regulation of VTA DA neuronal excitability has not been described.

In this study, we strove to find channel conductance which contribute to the

97 subthreshold depolarization and thus the spontaneous firing of the VTA DA neurons.
98 And furthermore, we investigated if these channels are the molecular mechanism for
99 the altered function activity of the VTA DA neurons related to depression-like
100 behaviors in mouse model of depression. We started by profiling the expression of
101 non-selective cation channels (NSCCs) of the VTA DA neurons using method of
102 Patch-Seq from midbrain DA neurons projecting to different brain regions, and then
103 focused on HCN, NALCN, TRPC6 and TRPV2 channels which are dominantly
104 expressed in these DA neurons.

105 **Results**

106 **Inflow of extracellular Na^+ contribute to the subthreshold depolarization of the**
107 **VTA DA neurons**

108 One key feature of the midbrain DA neurons is that these neurons are relatively
109 depolarized in the resting condition; the resting membrane potential (RMP) is far from
110 the K^+ equilibrium potential (~-55 mV *vs* ~-90 mV)[15], which enable the
111 spontaneous firing. Thus, there must be persistent inward depolarizing conductance
112 counterbalancing the hyperpolarizing K^+ conductance which otherwise would
113 maintain the RMP at a hyperpolarized level. The main aim of this study is to identify
114 the subthreshold depolarizing conductances which contribute to the spontaneous
115 firing of the VTA DA neurons. While we initially performed our experiments using
116 male mice, most of the electrophysiological experiments and some Western blot
117 experiments were also repeated using female mice, results of which were reported in
118 the following results. We first observed firing frequency and the RMP of the VTA DA
119 neurons using patch clamp recordings. The midbrain DA neurons, marked by
120 dopamine transporter (DAT), mainly located in the VTA and SNc (**Fig. 1Ai**). We also
121 performed single-cell PCR to identify the DA neurons with established markers for
122 DA neurons (TH, DAT, D_2R (type2 dopamine receptor), and GIRK2 (G protein-gated
123 inward rectifier K inwardly rectifying K^+ channels)). Although the majority of cells in
124 the VTA area are DA neurons (~60%), there are still about 30% GABA neurons and a
125 small number of glutamatergic neurons [37, 38]. Glutamatergic- and GABAergic
126 neurons were also single-cell PCR typed by using markers of VGluT2 (vesicular
127 glutamate transporter 2) and GAD1 (glutamic acid decarboxylase 1), respectively (**Fig.**

1Aii).

To focus on the intrinsic channel conductance for spontaneous firing, potential input modulation from fast-type transmitter transmission to the VTA DA neurons, namely activation of AMPA/kainite/NMDA receptor and $GABA_A$ receptor were blocked by receptor antagonists CNQX, APV and picrotoxin [15], respectively, in the following experiments.

We first studied whether inflow of extracellular Ca^{2+} contributed to initiation of spontaneous firing in the VTA DA neurons. It has been shown that, unlike the SNc DA neurons, the VTA DA neurons do not have subthreshold Ca^{2+} oscillatory waves[15], suggesting that subthreshold Ca^{2+} should not be an important component of subthreshold depolarizing conductance in the VTA DA neurons. In line with this finding, we found in our study, replacing Ca^{2+} with Mg^{2+} from the extracellular recording solution (ACSF, artificial cerebral spinal solution) did not reduce, but rather instead, increased the firing frequency of the VTA DA neurons in male and female mice (**Fig. 1B**, from 1.77 ± 0.14 Hz to 2.24 ± 0.18 Hz, n = 32, N = 16, Wilcoxon matched-pairs signed rank test, W = 526.0, $P < 0.0001$). Consistent with this，the RMP of the VTA DA neurons was not hyperpolarized by replacing Ca^{2+} with Mg^{2+} from ACSF (**Fig. 1C**, from -50.62 ± 0.62 mV to -49.49 ± 0.87 mV, n = 25, N = 15, Paired-sample T test, t = 2.368, df = 24, 95% CI: 0.1454 to 2.119, $P = 0.0263$).

We then, in comparison with Ca^{2+}, observed the role of extracellular Na^+ in the RMP of the VTA DA neurons. For this, we followed the method of a previous study[15], by replacing Na^+ in ACSF with NMDG (N-methyl-d-glucamine); TTX (Tetrodotoxin) was also added to block the TTX-sensitive Na^+ currents, which is known to be the main contributor to the suprathreshold depolarization component of the action potential. Replacement of the extracellular Na^+ with NMDG resulted in a hyperpolarization of the RMP in male and female mice (from -48.11 ± 0.99 mV to -59.93 ± 1.51mV, n = 17, N = 10, Paired-sample T test, t = 7.103, df = 16, 95% CI: -15.35 to -8.293, $P < 0.0001$, **Fig. 1D**), indicating a persistent inflow of Na^+ through a TTX-insensitive conductance which caused significant depolarization of the neurons, contributing significantly to the subthreshold depolarization of the VTA DA neurons. Taken together, above results indicate persistent Na^+ influx contribute to the

159 subthreshold depolarization of the VTA DA neurons.

160

161 **Potential candidates of channel conductance contributing to subthreshold**
162 **depolarization of the VTA DA neurons**

163 The channel conductance mediating the above-described persistent Na^+ influx should
164 come from a cation channel(s) permeating to Na^+. We thus investigated the presence
165 and expression level of non-selective cation channels (NSCCs) in the VTA DA
166 neurons using a combination of patch clamp and single-cell RNA-Seq (Patch-seq)
167 technology[39]. In this part of the study, we considered the heterogeneity and
168 projection-specificity of the VTA DA neurons, i.e. VTA DA neurons projecting to
169 different brain regions have different electrophysiological characteristics[40]. Using
170 retrograde labelling techniques by retrobeads, sixty male VTA neurons projecting to
171 five different brain regions (medial prefrontal cortex, mPFC; basal lateral amygdala,
172 BLA; nucleus accumbens core, NAc c; nucleus accumbens lateral shell, NAc ls;
173 nucleus accumbens medial shell, NAc ms) (**sFig.1**) were collected for RNA-Seq,
174 using patch-clamp electrodes. Consistent with previous study[40], the VTA DA
175 neurons projecting to above different brain regions were anatomically congregated
176 into subregions of the VTA (**sFig.2)**. The high expression of biomarkers (Tyrosine
177 hydroxylase, TH; Dopamine decarboxylase, Ddc and Dopamine transporter, DAT) in
178 the 45 cells of 60 cells (**Fig. 2A**) indicates that these are DA neurons. In addition,
179 fewer than half of sequenced DA neurons (predominantly those projecting to NAc ms,
180 BLA, and mPFC) have biomarkers (Vesicular glutamate transporter, VGluT1-3) of
181 glutamatergic neurons, predicting a possible coexistence of neurotransmitters (DA and
182 glutamate)[41].In contrast, fewer GABAergic neuronal markers (Glutamic acid
183 decarboxylase, GAD1/2 and vesicular GABA transporter, VGAT) co-expressed with
184 the DA neurons, which is consistent with previous studies that VTA DA neurons
185 which co-release GABA, contain low and even undetectable levels of GAD1, GAD2
186 and VGAT mRNA or protein[42, 43]. It needs to be noted that some neurons in the
187 VTA only expressed markers for glutamatergic or GABAergic neurons, these neurons
188 were excluded from further analysis as we focused our study on the DA neurons.

189 Expression levels of NSCCs in the VTA DA neurons classified by projection

specificity were analyzed and shown in **Fig. 2B**. Different colored strips on the top of the figure corresponded to the projection specificity coded by the same colors in **Fig. 2A**. Multiple transient receptor potential channels (TRP) were present in the VTA DA neurons, with prominent expression level of TRPC6 and TRPV2 (**Fig. 2Bi**). Other prominently expressed NSCCs included HCN2, HCN3, NALCN and pannexin 1 (Panx1) (**Fig. 2Bii**). Summarized averaged relative expression levels for eight most richly expressed NSCCs were shown in **Fig. 2Biii**. Furthermore, projection-specific expression of these dominantly expressed NSCCs were analyzed and shown in **Fig. 2C**; interestingly only TRPC6 seemed expressed in a projection-specific manner, namely, the VTA DA neurons projecting to the NAc have higher TRPC6 expression than the VTA DA neurons projecting to the BLA and the mPFC **(Fig. 2C**). In our subsequent study, we focused our study on HCN, NALCN, TRPC6 and TRPV2, one for they are the prominently expression channels, and two for some of these channels have been indicated in modulation of excitability of different neuron types[23, 24, 28-32, 44]. Panx1 was investigated in a separate study since it normally composes the semi channels which are different from these more conventional ion channels.

HCN does not contribute to the spontaneous firing of the VTA DA neurons

We mainly used two pharmacological tools as HCN channel blockers, CsCl and ZD7288[15, 24] to explore the role of HCN channels in the spontaneous firing of the male VTA DA neurons. Efficient blocking effect of these blockers on HCN channel was first verified. For this, the sag potential produced by a hyperpolarizing current (-100 pA) injection was used to assess HCN activity[24]. Both CsCl (3 mM) and ZD7288 (60 μM) effectively reduced the sag potential of VTA DA neurons in male mice (from 16.43 ± 2.96 mV to 3.84 ± 1.92 mV, n = 4, N = 4, Paired-sample T test, t = 4.246, df = 3, 95% CI: -22.03 to -3.155, P = 0.0239; from 19.38 ± 3.14 mV to 4.18 ± 2.60 mV, n = 4, N = 4, Paired-sample T test, t = 5.017, df = 3, 95% CI: -24.83 to -5.555, P = 0.0152, respectively) (**sFig. 3A and B**).

However, these same HCN blockers did not inhibit the spontaneous firing of the VTA DA neurons in male mice; CsCl slightly increased (1.96 ± 0.19 Hz to 2.14 ± 0.34 Hz, n = 7, N = 4, Paired-sample T test, t = 0.7171, df = 6, 95% CI: -0.4325 to 0.7911, P =

0.5003) whereas ZD7288 slightly decreased the firing frequency (1.65 ± 0.25 Hz to 1.50 ± 0.24 Hz, n = 13, N = 5, Paired-sample T test, t = 1.349, df = 12, 95% CI: -0.4033 to 0.09486, *P* = 0.2022), but none of these effects was statistically significant (*P* > 0.05) (**sFig. 3C and D)**. It has been reported that VTA DA neurons projecting to the NAc lateral shell have more pronounced HCN/Ih currents than other VTA DA neurons[40]. However, even the male VTA DA neurons projecting to the NAc lateral shell (retrogradely labelled by retrobeads), no effect of CsCl or ZD7288 on the spontaneous firing of the male VTA DA neurons were observed (from 2.04 ± 0.24 Hz to 1.93 ± 0.22 Hz, n = 5, N = 4, Paired-sample T test, t = 0.4798, df = 4, 95% CI: -0.7601 to 0.5361, *P* = 0.6564 by CsCl, and from 1.71 ± 0.29 Hz to 1.65 ± 0.33 Hz, n = 5, N = 5, Paired-sample T test, t = 0.4421, df = 4, 95% CI:-0.4368 to 0.3168, *P* = 0.6813 by ZD7288) (**sFig. 4A and B**).

HCN are activated by membrane hyperpolarization, with an activation threshold around -70~-90 mV (HCN2, HCN3)[45, 46]. At a depolarized RMP like these in the VTA DA neurons (-51.28 ± 1.85 mV, n = 8, N=8; e.g. -54.50 mV, **sFig. 3Ai**, and -53.50mV, **sFig. 3Bi**), HCN are most likely not activated thus would not participate in generation of spontaneous firing. To further prove this, we tested if a more hyperpolarized RMP would involve HCN in the spontaneous firing of the VTA DA neurons. For this, we first lowered the K^+ concentration in the extracellular ACSF from 3 mM to 1.5 mM to increase the gradient between inside and outside cellular K^+; this maneuver indeed hyperpolarized the cell membrane from -49.45 ± 0.93 mV to -62.95 ± 2.56 mV (n = 7, N = 7, Paired-sample T test, t = 6.373, df = 6, 95% CI: -18.69 to -8.318, *P* = 0.0007) (**sFig. 4C**). Interestingly, under 1.5 mM extracellular K^+, the spontaneous firing of the male VTA DA neurons was almost totally blocked by ZD7288 (**sFig. 4D**), although an initial enhancement was seen in some neurons (**sFig. 4Di**).

We tested another possible mechanism for HCN's failure to participate in generation of VTA DA firing. It has been reported that in the midbrain SNc DA neurons, HCN is involved in the spontaneous firing in young but not in adult mice, due to a more hyperpolarization-shifted activation threshold of HCN in SNc DA neurons in adult mice. We tested if this could also be the case in the VTA DA neurons. Indeed, as

shown in **sFig. 4E**, in contrast to what we saw in adult male mice, the spontaneous firing frequency of the VTA DA neurons in young male mice (less than 15 days postnatal) was significantly reduced by ZD7288 (from 1.86 ± 0.29 Hz to 0.98 ± 0.24 Hz, n = 9, N = 5, Paired-sample T test, t = 3.345, df = 8, 95% CI: -1.487 to -0.2734, P = 0.0101).

Taken together, above results suggest HCN is not involved in the spontaneous firing of the VTA DA neurons in adult male mice, due to a depolarized RMP and a hyperpolarization-shifted activation property.

NALCN contributes to subthreshold depolarization and spontaneous firing of the VTA DA neurons

The Na^+ currents produced by NALCN have been suggested to be an important component of background Na^+ currents in multiple central neurons including DA neurons in the substantia nigra[28].We next investigated if NALCN also play a role in setting the RMP and in the spontaneous firing of the VTA DA neurons. Consistent with above RNA-Seq results, both immunofluorescence (**Fig. 3A**) and single-cell PCR (**Fig.3B)** results confirmed broad expression of NALCN in the VTA DA neurons.

$GdCl_3$ (100 μM), a non-selective NALCN blocker [30, 31], hyperpolarized the RMP of the male VTA DA neurons from -48.88 ± 2.41 mV to -68.88 ± 1.28 mV (n = 7, N = 7, Paired-sample T test, t = 11.38, df = 6, 95% CI: -24.30 to -15.70, P < 0.0001) (**Fig. 3C**), reduced the spontaneous firing frequency of the male VTA DA neurons from 1.89 ± 0.29 Hz to 1.32 ± 0.37 Hz (n = 7, N = 3, Paired-sample T test, t = 5.711, df = 6, 95% CI: -0.8183 to -0.3274, P = 0.0012) (**Fig. 3D**). L703,606 (10 μM), a selective NALCN blocker[32], also hyperpolarized the RMP of the male VTA DA neurons from -49.61 ± 1.48 mV to -54.30 ± 1.67 mV (n = 6, N = 4, Paired-sample T test, t = 14.95, df = 5, 95% CI:-5.498 to -3.885, P < 0.0001) **(Fig. 3E)**, reduced the spontaneous firing frequency of the male and female VTA DA neurons from 1.87 ± 0.23 Hz to 0.34 ± 0.14 Hz (n = 20, N = 10, Wilcoxon matched-pairs signed rank test, W = -210.0, P < 0.0001) (**Fig. 3F**).

To observe a more specific effect on NALCN, a shRNA against NALCN was used to

283 knockdown NALCN. For this, AAV9 viral construct
284 (AAV9-U6-shRNA(NALCN)-CMV-GFP) was injected into the VTA of a mouse;
285 similar AAV viral construct containing scramble-shRNA of nonsense sequences was
286 utilized as controls. The qPCR results show sufficient knockdown of NALCN mRNA
287 (NALCN-shRNA: 0.32 ± 0.07, N = 6; control scramble-shRNA: 1.07 ± 0.19, N = 6,
288 Two-sample T test, t = 3.714, df = 10, 95% CI: -1.200 to -0.3000, P = 0.0040, **Fig.**
289 **3G**) in the VTA tissue. Immunofluorescence results (**Fig. 3H**) show efficient infection
290 of the VTA DA neurons (GFP expression in the DAT-positive neurons) by the virus.
291 Knockdown of NALCN in the VTA DA neurons by shRNA almost completely
292 silenced the firing of the male and female VTA DA neurons (0.08 ± 0.02 Hz *vs* 1.60 ±
293 0.15 Hz in NALCN-shRNA (n = 35, N = 8) and scramble-shRNA (n = 30, N = 8)
294 infected VTA DA neurons, respectively, Mann-Whitney U test, U = 0, $P < 0.0001$, **Fig.**
295 **3I**).Furthermore, the RMP of the male VTA DA neurons was significantly
296 hyperpolarized (-62.13 ± 1.00 mV *vs* -50.86 ± 0.57 mV in NALCN-shRNA and
297 scramble-shRNA infected VTA DA neurons, respectively, n = 18 and 15, N = 5 and 5,
298 Mann-Whitney U test, U = 0, $P < 0.0001$, **Fig. 3J**).
299 Taken together, above results suggest that NALCN is a major contributor to the
300 subthreshold depolarization and contribute significantly to the generation of
301 spontaneous firing in the VTA DA neurons.
302
303 **TRPC6 contributes to subthreshold depolarization and spontaneous firing of the**
304 **VTA DA neurons**
305 Above RNA-Seq results suggest a broad and strong expression of TRPC6 and TRPV2
306 channels in the VTA DA neurons. This part of the experiments was focused on the
307 role of these two TRP channels in subthreshold depolarization and spontaneous firing
308 of the VTA DA neurons.
309 Consistent with the RNA-Seq results, single-cell PCR experiments confirmed high
310 proportion expression of TRPC6 and TRPV2 in the VTA DA neurons (**Fig. 4A**);
311 among the 28 VTA DA neurons (DAT^+), 20 neurons expressed TRPV2 (71.4%), and
312 18 neurons (64.3%) expressed TRPC6. TRPC3, which is highly homologous with
313 TRPC6[47] and has been reported to be involved in the firing activity of the SNc DA

314 neurons[32], was neither detected in RNA-Seq study (**Fig. 2B**), nor in the single-cell
315 PCR experiment (**Fig. 4A**). These results reciprocally confirmed the reliability of both
316 RNA-Seq and single cell PCR results.
317 General roles of TRP channels in subthreshold depolarization and spontaneous firing
318 of the VTA DA neurons were first assessed using a non-selective broad-spectrum TRP
319 channel blocker, 2-aminoethoxydiphenylborane (2-APB; 100 μM) and a selective
320 TRPC6 channel blocker, larixyl acetate[48] (LA; 10 μM). Both blockers significantly
321 reduced the firing frequency of the VTA DA neurons (2-APB for male mice: from
322 1.32 ± 0.27 Hz to 0.06 ± 0.02 Hz, n = 12, N = 5, Wilcoxon matched-pairs signed rank
323 test, W = -78.0, P = 0.0005; LA for male and female mice: from 1.59 ± 0.26 Hz to
324 0.55 ± 0.15Hz, n = 14, N = 8, Wilcoxon matched-pairs signed rank test, W = -105.0, P
325 = 0.0001; **Fig. 4B, 4C**). Accordingly, both blockers also significantly hyperpolarized
326 the RMP of the male and female VTA DA neurons (2-APB: from -49.97 ± 1.29 mV to
327 -59.27 ± 1.22 mV, n = 10, N = 9, Paired-sample T test, t = 8.082, df = 9, 95% CI:
328 -11.90 to -6.693, P < 0.0001; LA: from -53.41 ± 0.81 mV to -57.82 ± 1.13 mV, n = 9,
329 N = 7, Paired-sample T test, t = 6.431, df = 8, 95% CI: -5.993 to -2.829, P = 0.0002;
330 **Fig. 4D, 4E**).
331 We then tested a more TRPV channel-selective blocker ruthenium red (RR), to study
332 possible role of TRPV2 (and other TRPV) in the spontaneous firing of the VTA DA
333 neurons. RR (60 μM), on average statistically, did not affect the spontaneous firing of
334 the male VTA DA neurons (from 2.30 ± 0.31 Hz to 2.18 ± 0.31 Hz, n = 9, N = 6,
335 Paired-sample T test, t = 0.4486, df = 8, 95% CI: -0.7621 to 0.5139, P = 0.6656) (**sFig.
336 5**). However, it needs to be noted that among the nine VTA DA neurons we tested,
337 both increase (**sFig. 5B**) and decrease (**sFig. 5C**) of firing frequency by RR were seen,
338 thus with opposite changes of firing frequency in different populations of neurons
339 (**sFig. 5A**), no overall effect of RR was obtained from the current analysis.
340 We then focused our next study on TRPC6. Consistent with both RNA-Seq (**Fig. 2B**)
341 and single-cell PCR (**Fig. 4A**) results, the mRNA level of TRPC6 in mPFC-projecting
342 VTA single DA neuron is significantly lower than that in NAc c-projecting VTA
343 single DA neuron (0.56 ± 0.12, n = 25, N = 8 for mPFC-projecting TH-positive cells
344 *vs* 1.09 ± 0.10, n = 28, N = 7 for NAc c-projecting TH-positive cells, Mann-Whitney

U test, U = 173, P = 0.0013, **Fig. 5A**) The immunofluorescence results also demonstrated strong expression of TRPC6 protein in the VTA DA neurons (**Fig. 5B**, TH-positive). A AAV viral construct with shRNA against TRPC6 (AAV9-U6-shRNA(TRPC6)-CMV-GFP) was injected into the VTA of mice, to knockdown TRPC6; efficiency of this knockdown was assessed by using qPCR measuring the mRNA level of TRPC6 in the VTA tissue (**Fig. 5C**), and efficiency of viral infection into the VTA DA neurons (marked by DAT) was observed through visualization of GFP (**Fig. 5D**). Both qPCR (**Fig.5C**) and immunofluorescence (**Fig. 5D**) results indicated a sufficient repression of TRPC6 in the VTA DA neurons. Indicative of a significant role in the spontaneous firing and subthreshold depolarization, knockdown of TRPC6 (TRPC6-KD) resulted in a substantial reduction in the spontaneous firing frequency (0.43 ± 0.07 Hz, n = 37, N = 12 for TRPC6-KD *vs* 1.88 ± 0.16 Hz, n = 27, N = 11 for scramble-shRNA, Mann-Whitney U test, U = 48, P < 0.0001,for male and female mice, **Fig. 5E**), and hyperpolarization of the RMP (-58.32 ± 1.77 mV, n = 10, N = 6 for TRPC6-KD *vs* -50.24 ± 0.65 mV, n = 10, N = 6 scramble-shRNA, Mann-Whitney U test, U = 8, P = 0.0007, for male mice, **Fig. 5G**) of the VTA DA neurons. In addition, the inhibitory effect of 2-APB and LA on the firing of VTA DA neurons infected with TRPC6-shRNA largely diminished, with no statistical difference in firing frequency before and after dosing (2-APB: from 0.58 ± 0.15 Hz to 0.40 ± 0.15 Hz, n = 7, N = 5, Wilcoxon matched-pairs signed rank test, W = -18.00, P = 0.1563, for male mice, **Fig. 5F**; LA: from 0.43 ± 0.05 Hz to 0.43 ± 0.06 Hz, n = 8, N = 5, Paired-sample T test, t = 0.000, df = 7, 95% CI:-0.05740 to 0.05740, P > 0.9999, for male mice, **Fig. 5H**).

Consequence of knocking down TRPC6 described above should not be a result of a secondary effect on other TRPC channels with which TRPC6 is known to interact to form heteromers, such as TRPC4 and TRPC7[49, 50], since in experiments using single cell PCR (**sFig. 6A**), it was found only a very small proportion of TRPC6-positive DA cells ($TRPC6^{+}DAT^{+}$) expressed TRPC4 (**sFig. 6Bi**) or TRPC7 (**sFig. 6Bii**), in consistent with the results of single-cell RNA-seq results (**Fig. 2**).

Taken together, above results indicate TRPC6 is an important contributor in subthreshold depolarization and spontaneous firing of the VTA DA neurons.

376

377 **Down-regulation of TRPC6 contributes to the altered firing activity of the VTA**
378 **DA neurons in depression model**

379 In multiple depression models, the depression-like behavior was directly linked to the
380 altered firing activity of the VTA DA neurons[4, 7, 51-53]. In consideration of the
381 evidence we described above that NALCN and TRPC6 play key roles in firing
382 activity of the VTA DA neurons, we went further to study if these channels also
383 contributed to the altered firing activity of the VTA DA neurons and to the
384 development of the depression-like behavior in depression models of mice.

385 We first established a mice depression model of chronic mild unpredictable stress
386 (CMUS) [54], which, after 5 weeks subjecting to two different stressors every day
387 (**Fig. 6A**), manifested chronic-stress-induced depression-like behaviors in the sucrose
388 preference test (SPT) and the tail suspension test (TST), with reduced sucrose
389 preference and lengthened immobility time, respectively (male mice: **Fig. 6B**, female
390 mice: **sFig. 8B, I**). Multiple other behaviors tests were also performed on these
391 CMUS male and female mice (male mice: **sFig. 7**, female mice: **sFig. 8A, C-H**), all
392 indicating depression/anxiety-like behaviors.

393 It has been shown that a reduced firing activity in the VTA DA neurons is responsible
394 for the chronic-stress-induced depression-like behavior in the CMUS model[53, 55].
395 Consistent with this finding, we also found the firing frequency of the VTA DA
396 neurons from the CMUS male and female mice was significantly reduced as
397 compared with that from the control male and female mice (2.90 ± 0.17 Hz, n = 53, N
398 = 31 for control mice *vs* 1.24 ± 0.08 Hz, n = 68, N = 33 for CMUS mice,
399 Mann-Whitney U test, U = 415, $P < 0.0001$, **Fig. 6C**). In agreement with a role for
400 TRPC6 in this reduced firing activity, TRPC6 protein in the VTA tissue of male and
401 female CMUS mice was found to be down-regulated in western blot experiments (**Fig.**
402 **6D**). On the other hand, NALCN protein in the VTA was not altered in the CMUS
403 male mice model of depression (**sFig. 9**).

404 We also tested if this down-regulation of TRPC6 protein could also be found in a
405 similar but different model of depression. For this, a chronic restraint stress (CRS)
406 model was used. After 3 weeks of restraint stress stimulation, the CRS male mice

407 developed similar depression/anxiety-like behavior in the behavior tests like these
408 similarly performed in the CMUS model (**sFig. 10A-I**). Importantly, male mice with
409 CRS-induced depression also showed a significant downregulation of TRPC6 protein
410 in the VTA (0.38 ± 0.06 fold, N = 10 for control and N = 14 for CRS, Two-sample T
411 test, t = 7.369, df = 22, 95% CI: -0.8006 to -0.4489, $P < 0.0001$, **sFig. 10J**).
412 It is known that the activity of VTA dopamine neurons that project to mPFC is
413 decreased in CMUS mice with depressive behaviors[11, 53]. Assuming that the
414 decreased firing activity of the mPFC-projecting VTA DA neurons in the CMUS mice
415 was associated with the down-regulation of TRPC6 expression, we reasoned that the
416 firing activity in these CMUS mice would respond less to the TRP channel inhibitors.
417 Indeed, TRP channel inhibitor 2-APB and TRPC6 inhibitor LA decreased their
418 inhibitory effect on the firing activity of the mPFC-projecting VTA DA neurons from
419 the CMUS male and female mice (2-APB:1.56 ± 0.15Hz to 1.19 ± 0.14 Hz, n = 25, N
420 = 15, Kruskal-Wallis test, $P > 0.9999$; LA: 1.12 ± 0.11Hz to 0.83 ± 0.08 Hz, n = 30,
421 N = 18, Kruskal-Wallis test, $P > 0.9999$) compared with these from the control mice
422 (2-APB: 3.35 ± 0.29 Hz to 0.17 ± 0.08 Hz, n = 22, N = 15, Kruskal-Wallis test, $P <$
423 0.0001; LA: 2.97 ± 0.16 Hz to 0.17 ± 0.08 Hz, n = 25, N = 16, Kruskal-Wallis test, P
424 < 0.0001) (**Fig. 6E** and **F**).
425 Taken together, above results suggest down-regulation of TRPC6 results in the altered
426 firing activity of the VTA DA neuron in mice models of depression**.**
427
428 **Down-regulation of TRPC6 in the VTA DA neurons confer the mice with**
429 **depression-like behavior**
430 If down-regulation of TRPC6 is crucial for the depression-like behaviors, like that
431 indicated above in the CMUS and the CRS depression models, the down regulation of
432 TRPC6 in non-stressfully treated mice should also develop depression-like behavior.
433 We tested this possibility by selectively knocking down TRPC6 in the VTA DA
434 neurons, using DAT-Cre male mice injected with a AAV viral construct
435 (AAV9-hSyn-DIO-shRNA (TRPC6) -RFP) (**Fig. 7A**), driving the expression of
436 shRNA against TRPC6 selectively in the VTA DA neurons. Three weeks after the
437 AAV injection, the qPCR (**Fig. 7B**) and the immunofluorescence results (**Fig. 7C**)

438 indicated an efficient down-regulation of TRPC6 in the VTA DA neurons.

439 We next compared the depression- and anxiety-like behaviors in these conditionally
440 TRPC6-knockdown male mice (TRPC-cKD) with that in the control mice (infected
441 with virus carrying the scrambled shRNA). As shown in **Fig. 7D**, in the TRPC6-cKD
442 male mice, the sucrose preference was significantly reduced (7Di, 74.52 ± 2.00 %, N
443 = 10 for TRPC6-cKD, *vs* 85.87 ± 1.85 %, N = 10 for control, Two-sample T test, t =
444 4.172, df = 18, 95% CI: -17.07 to -5.634, P = 0.0006), the immobility time in the Tail
445 suspension test was significantly lengthened (7Dii, 142.00 ± 4.66 s *vs* 121.40 ± 3.94 s,
446 Two-sample T test, t = 3.377, df = 18, 95% CI: 7.785 to 33.41, P = 0.0034). In the
447 elevated plus maze test, the percentage of time spent in the open arm was significantly
448 reduced (7Diii, 1.60 ± 0.50 % *vs* 11.42 ± 2.04 %, Mann-Whitney U test, U = 2, P <
449 0.0001) and the percentage of time spent in the closed arm was also significantly
450 increased (7Div). And the Cre-dependent TRPC6-overexpression in male VTA
451 DAT-Cre mice (TRPC6-cOE) rescued the selective-TRPC6-knockdown-induced
452 depression-like behaviors (**Fig. 7E-H**). Furthermore, selectively knockdown of
453 TRPC6 in the mPFC-projecting VTA DA neurons (virus-retro carrying
454 DIO-TRPC6-shRNA (TRPC6-rcKD) was injected into the mPFC of DAT-Cre male
455 mice) (**Fig. 8A-C**) also conferred the mice with the depression- and anxiety-like
456 behaviors (**Fig. 8D**).

457 Taken together, these results suggest down-regulation of TRPC6 in the VTA DA
458 neurons promotes the phenotypes of depression/anxiety of the mice in the CMUS.

459

460 ## Discussion

461 In this study, we made a systematic study on the molecular mechanism for the
462 subthreshold depolarization that drive spontaneous firing of the VTA DA neurons. We
463 identified TRPC6 channels, alongside NALCN, as major contributors to this
464 subthreshold depolarization and related spontaneous firing, and further importantly,
465 we also demonstrated that TRPC6 contributed to the altered firing activity of the VTA
466 DA neurons under states of chronic-stress-induced depression-like behaviors.

467 The nature of a relatively depolarized resting membrane potential in the VTA DA
468 neurons imposes a need for a full understanding of the channel conductance

469 underlying this depolarization. It is first clear from these current and previous studies
470 that this conductance is mediated by a persistent Na^+ influx. Unlike the DA neurons in
471 the SNc, where Ca^{2+} influx is needed for the spontaneous firing [56], the results in our
472 and others' studies indicate that Ca^{2+} influx are not necessary for the spontaneous
473 firing of the VTA DA neurons. Replacement of Ca^{2+} ions in the extracellular fluid
474 with Mg^{2+} accelerates the frequency of spontaneous firing (Fig. 1B) [15], possibly
475 resulting from a reduced activity of the Ca^{2+}-activated K^+ currents and an increased
476 activity of NALCN[28, 57]. Consistent with this, removing extracellular Ca^{2+} did not
477 hyperpolarize the RMP, which verifies more precisely for a role of Ca^{2+} influx on the
478 subthreshold depolarization. On the other hand, consistent the previous study [15], a
479 TTX-insensitive Na^+ influx clearly contributed to the subthreshold depolarization (Fig.
480 1D).
481 A TTX-insensitive nature of this Na^+ conductance suggests that cation conductance
482 permeable to Na^+ might be the molecular candidates. We first focused on the HCN
483 channels because, (1) it has been suggested HCN channels are important regulators
484 for the spontaneous firing of VTA DA neurons in adult male mice under states of
485 depression-like behaviors[7, 11]; (2) HCN are one of the more highly expressed
486 NSCCs in the VTA DA neurons in our single cell RNA-Seq study; (3) HCN are
487 permeable to Na^+[58]. However, it is clear from our study that HCN does not
488 contribute to the spontaneous firing of the VTA DA neurons in the adult male mice;
489 none of the known HCN blockers we used had any significant effects on the firing
490 activity. Presence of HCN has long been used as a signature of DA neurons[59], also
491 as a differentiating factor for the projection-specificity of the VTA DA neurons[40].
492 Nonetheless, contribution of HCN to the spontaneous firing of the VTA DA neurons
493 has been controversial; the HCN blockers ZD7288 and CsCl have been reported as
494 both effective[23, 24, 60] and non-effective [15] on the spontaneous firing of the VTA
495 DA neurons. A closer inspection into our and others' results present a possible
496 explanation for these different results: in the younger rodents (less than one month old
497 [61] and less than 15 days old in our study), the HCN in the DA neurons play a more
498 important role whereas in the adult mice (~ 8 weeks [61]), like the male adult ones

499 (6~8 weeks) we used in this study, the HCN do not contribute to the spontaneous
500 firing of the VTA DA neurons. This is likely due to a shift of activation gating of HCN
501 channels in a hyperpolarization direction with age, thus the modulation of HCN on the
502 firing activity diminishes with age, as it is described in the SNc DA neurons[61].
503 Consistent with this, we found hyperpolarizing the RMP rendered the VTA DA
504 neurons of the adult male mice with sensitivity to the HCN blockers. Thus, the VTA
505 DA neurons in adult male mice do not use HCN to depolarize the membrane to
506 generate action potentials.
507 NALCN is widely expressed in central neurons[62, 63], and is a popular candidate
508 considered for the ion mechanism of the subthreshold depolarization currents and Na^+
509 leaky currents. NALCN has been shown to be an important component of background
510 Na^+ currents and to be important for neuronal excitability in the hippocampal neurons,
511 posterior rhomboid nucleus (Retrotrapezoid nucleus/RTN) chemo-sensitive neurons
512 (CO_2/H^+-sensitive neurons), GABA neurons and DA neurons in the substantia nigra,
513 and spinal projection neurons [28-32, 44]. Our results with single cell RNA-Seq,
514 single-cell PCR and immunofluorescence methods validated high level expression of
515 NALCN in the VTA DA neurons; both the pharmacological and the
516 NALCN-gene-knockout experiments demonstrated convincingly involvement of
517 NALCN in subthreshold depolarization and spontaneous firing of the VTA DA
518 neurons.
519 We did not detect alteration of NALCN protein expression in the depression model of
520 CMUS in the VTA tissue. However, this does not completely exclude a possible
521 contribution of NALCN to the altered functional activity of the VTA DA neurons
522 which underlies the chronic-stress-induced depression-like behaviors. Future study
523 focusing on the functional property of NALCN in the cellular level of the VTA DA
524 neurons under a state of depression is needed to clarify this issue. NALCN is after all
525 a potential drug target in consideration of its important contribution to the resting
526 membrane potential and functional activity of neurons.
527 The most interesting and important finding of this study is the role of TRPC6 in
528 regulation of the firing activity of the VTA DA neurons in both physiological and

529 depression-state conditions, and its involvement in depression-like behaviors; the
530 experimental evidence from pharmacological, gene silencing, electrophysiological
531 and behavior results unambiguously support this conclusion. It is interesting to note,
532 although with an unclear neuronal circuit mechanism of action, the TRPC6 channel
533 opener hyperforin was previously reported to have antidepressant effects in
534 corticosterone-depressed mice, which were reversed by prior administration of the
535 TRPC6 blocker larixyl acetate[64]. Also, in a CMUS rat model, TRPC6 expression
536 was found to be downregulated in the hippocampus, and administration of the TRPC6
537 opener hyperforin was effective in alleviating depression-like behavior[65]. Our study
538 provides strong and convincing evidence that TRPC6 is a key regulator of the VTA
539 DA neurons which are known to be a key player in depression states [7, 21, 51, 52,
540 66].
541 The above-mentioned role for TRPC6 should come from its contribution to the
542 subthreshold depolarization, through a persistent permeation to the influx of Na^+.
543 Although TRPC channels has been better recognized for their permeability to Ca^{2+}
544 and their regulation on cellular Ca^{2+} homeostasis, the importance of TRPC channels
545 for the permeability of monovalent cations, especially Na^+, is now gradually being
546 appreciated [67]. In the substantial nigra GABA and DA neurons, TRPC3 has been
547 reported to play an important role in maintaining depolarization membrane potential,
548 peacemaking, and firing regularity[32, 34]. Otherwise, it has been reported that slow
549 tonic firing of SNc DA neurons, depends on the basal activity of both the NALCN and
550 TRPC3 channels, but that burst firing does not require TRPC3 channels but relies
551 only on NALCN channels[68]. TRPC6 and TRPC3 belong to the same TRPC family
552 subclass and TRPC6 is more than 75% homologous to TRPC3[47]. Interestingly, our
553 results with single-cell RNA-Seq and single-cell PCR demonstrated the rich
554 expression of TRPC6 in the VTA DA neurons among all TRP channels but no
555 expression of TRPC3 was found in these neurons. These results present an
556 opportunity for selectively targeting a single TRPC channel to exert selective
557 pharmacological results. Besides, TRPC4 expression was detected in a uniformly
558 distributed subset of rat VTA DA neurons[36], which differs with our results with

559 single-cell RNA-Seq and single-cell PCR, and TRPC4 KO rats showed decreased
560 VTA DA neuron tonic firing and deficits in cocaine reward and social
561 behaviors[36].TRPC4 is detected to be expressed with a low level in the VTA DA
562 neurons of male mice by single-cell RNA-Seq (Fig.2) and in TRPC6 and DAT
563 double-positive VTA cells by single-cell PCR (sFig.6).The different species used in
564 this and our study may be one explanation, but the role of TRPC4 in the excitability
565 of mice VTA TRPC6-negative DA neurons is worth to investigating further.
566 It has also been demonstrated in cell types other than neurons, such as rat portal vein
567 smooth muscle cells, the activation of α-adrenergic receptor can open TRPC6, which
568 leads to cell depolarization, activation of voltage-dependent Ca^{2+} channels, and
569 ultimately the contraction of smooth muscle cell[69]; it is also shown that angiotensin
570 II and endothelin I can activate TRPC3/C6 heterodimers via vascular G
571 protein-coupled receptors (GPCR), thereby depolarizing cells [70, 71]. Following this
572 line, it would be very interesting to know if TRPC6 in the VTA DA neurons, where
573 multiple GPCR reside receiving input and auto modulation by neuronal transmitters
574 [72, 73], could also be a target of modulation with similar mechanism. In
575 consideration of the important role, we described here in this study, this type of
576 modulation will present possible explanations for some unsolved mechanism for
577 physiological and pathophysiological functions of the VTA DA neurons.
578 The facts that down-regulation of TRPC6 proteins was correlated with reduced firing
579 activity of the VTA DA neurons as well as the chronic-stress-induced depression-like
580 behaviors of mice with both sexes, and that knocking down of TRPC6 in the VTA DA
581 neurons confers the male mice with depression-like behaviors strongly suggest a
582 crucial role for TRPC6 in the development of chronic-stress-induced depression-like
583 behaviors under stressful conditions like CMUS. To reinforce this, down-regulation of
584 TRPC6 was also found in another chronic-stress-induced depression model of CRS, a
585 model with similar neuronal alteration of reduced firing activity in the VTA DA
586 neurons to that described in the CMUS model[74]. These facts with the fact that
587 TRPC6 activator hyperforin is an effective antidepressant in multiple depression
588 models[64, 65], and that hyperforin is the principal component of St. John's wort, a

589 well-known antidepressant herb[75], present TRPC6 as a very attractive drug target
590 for new lines of antidepressants.

591 **Materials and methods**

592

593 **Animal Preparation**

594 Male or female 6-8-week-old C57BL/6 (Vital River, China) and DAT-Cre mice with a
595 C57BL/6 background (Stock No: 006660, the Jackson Laboratories, USA) were used
596 for the studies. Ethics Statement: All experiments were conducted in accordance with
597 the guidelines of Animal Care and Use Committee of Hebei Medical University and
598 approved by the Animal Ethics Committee of Hebei Medical University (Shijiazhuang,
599 China), 2017013.

600 **Brain slice preparation**

601 The details for the preparation of coronal brain slice containing VTA were the same as
602 described in our previously published work[21, 72]. Briefly, mice were anesthetized
603 with chloral hydrate (200 mg/kg, i.p.). After intracardial perfusion with ice-cold
604 sucrose solution, the brains of the mice were removed quickly and placed into the
605 slicing solution. The ice-cold sucrose-cutting solution contained (in mM): sucrose 260,
606 $NaHCO_3$ 25, KCl 2.5, NaH_2PO_4 1.25, $CaCl_2$ 2, $MgCl_2$ 2, and D-glucose 10;
607 osmolarity, 295-305 mOsm). Using the vibratome (VT1200S; Leica, Germany), the
608 coronal midbrain slices (250 μm-thick) containing VTA were sectioned. The slices
609 were incubated for 30 min at 36°C in oxygenated artificial cerebrospinal fluid (ACSF)
610 (in mM: NaCl 130, $MgCl_2$ 2, KCl 3, NaH_2PO_4 1.25, $CaCl_2$ 2, D-Glucose 10, $NaHCO_3$
611 26; osmolarity, 280-300 mOsm), and were then left for recovery for 60 min at room
612 temperature (23-25°C) until use.
613 The brain slices were transferred to the recording chamber and were continuously
614 perfused with fully oxygenated ASCF during recording.

615 **Identification of DA neurons and electrophysiological recordings**

616 Recordings in the slices were performed in whole-cell current-clamp and

617 voltage-clamp configurations on the Axoclamp 700B preamplifier (Molecular Devices,
618 USA) coupled with a Digidata 1550B AD converter (Molecular Devices, USA).
619 Neurons in the VTA were visualized with a 40× water-immersion objective equipped
620 by an optiMOS microscope camera (Qimaging, Canada) on an Olympus-BX51
621 microscope (Olympus, Japan). Projection-specific or GFP-positive VTA neurons were
622 identified by infrared-differential interference contrast (IR-DIC) video microscopy
623 and epifluorescence (Olympus, Japan) for detection of retrobeads (red) positive or
624 GFP-positive neurons.
625 For whole-cell recording, glass electrodes (3-5 MΩ) were filled with internal solution
626 (in mM): K-methyl sulfate 115, KCl 20, $MgCl_2$ 1, HEPES 10, EGTA 0.1, MgATP 2
627 and Na_2GTP 0.3, pH adjusted to 7.4 with KOH. And the extracellular solution was the
628 ACSF.
629 In whole-cell current-clamp mode, HCN function was judged by the inwardly
630 rectifying characteristic sag potential generated by giving a hyperpolarizing current
631 (-100 pA).
632 When recording the effect of removing extracellular Ca^{2+} on spontaneous cell
633 discharge, $CaCl_2$ in the ACSF was replaced with $MgCl_2$, and the final $MgCl_2$
634 concentration was 4 mM.
635 The resting membrane potential (RMP) was measured in current clamp mode (I = 0);
636 the composition of the recording solution (mM) contained: NaCl 151, KCl 3.5, $CaCl_2$
637 2, $MgCl_2$ 1, glucose 10, and HEPES 10, and the pH was adjusted to about 7.35 with
638 NaOH. 1 μM tetrodotoxin was added to the extracellular solution to abolish action
639 potential during measurement of the RMP.
640 To observe the effect of extracellular Na^+ on the RMP, NaCl in the original recording
641 solution was replaced with equimolar NMDG, and the NMDG-recording solution
642 (mM) contained: NMDG 151, KCl 3.5, $CaCl_2$ 2, $MgCl_2$ 1, glucose 10, and HEPES 10,
643 and the pH was adjusted to 7.35 with KOH.
644 For recording spontaneous firing of the neurons, cell-attached "loose-patch" (100-300
645 MΩ) recordings were used[76]. In this case, patch-pipettes (2-4 MΩ) were filled with
646 ACSF, and the spontaneous activity was recorded in the current-clamp mode (I = 0).
647 The synaptic blockers (CNQX, 10 μM; APV, 50 μM and gabazine, 10 μM) were

648 added to isolate the intrinsic firing properties.
649 At the end of electrophysiological recordings, the recorded VTA neurons were
650 collected for single-cell PCR.VTA DA neurons were identified by single-cell PCR for
651 the presence of TH and DAT.
652
653 **Retrograde labelling**
654 Briefly, under general chloral hydrate anaesthesia (200 mg/kg, i.p.) and stereotactic
655 control (RWD Instruments, Guangzhou, China), the skull surface was exposed. All
656 coordinates are relative to bregma in mm using landmarks and neuroanatomical
657 nomenclature that was described in the Franklin and Paxinos mouse brain atlas[77] .
658 Red retrobeads (100 nl for single injection; Lumafluor Inc., Naples, FL, USA) were
659 injected into the following sites by KD scientific syringe pump (KD scientific,
660 Holliston MA, USA): bilaterally into NAc core (NAc c), NAc lateral shell (NAc ls),
661 NAc medial shell (NAc ms) and basolateral amygdala (BLA), 4 separate sites (2 per
662 hemisphere) into medial prefrontal cortex (mPFC). Coordinates for infusions were as
663 follows: NAc c (AP +1.50, ML ±0.84, DV -4.00~-3.80; 100 nl beads); NAc ls (AP
664 +0.86, ML ±1.72, DV -4.24~-3.93; 100 nl beads); NAc ms (AP +1.70, ML ±0.53, DV
665 -4.16~--3.60; 100 nl beads); mPFC (AP +2.05 and 2.15, ML ±0.27, DV -2.26~-1.70;
666 200 nl beads); BLA (AP -1.46, ML ±2.85, DV -4.01~-3.58; 100 nl beads). Retrobeads
667 were delivered through a pulled glass pipette using a PAP107 Multipipette Puller
668 (MicroData Instrument, Inc., USA) and at a rate of 100 nl/min; the injection needle
669 was left in place for at least 5 minutes after each infusion. Following surgery, mice
670 were returned to single housing. For sufficient labelling, survival periods for
671 retrograde tracer transport depended on respective injection areas: NAc c, NAc ls,
672 NAc ms, 14 days; mPFC, 21 days; BLA 14 days[40]. Coronal sections of injection
673 sites were stained with 4, 6-diamidino-2-phenylindole (DAPI, Sigma, USA) to
674 confirm representative target location. Then, serial analyses of the injection-sites were
675 carried out routinely.
676
677 **AAV for gene knockdown or overexpression and viral construct and injection**
678 For knockdown of NALCN and TRPC6, AAV9-U6-shRNA(NALCN)-CMV-GFP

679 (300 nl) or AAV9-U6-shRNA(TRPC6)-CMV-GFP or its control
680 AAV9-scramble-shRNA was delivered into the VTA (AP -3.08 mm; ML ±0.50 mm;
681 DV -5.00~-4.20 mm) of the mice. AAV9-hSyn-DIO-shRNA(TRPC6)-RFP (300 nl) or
682 its control AAV9-scramble-shRNA was delivered into the VTA of the DAT-Cre
683 C57BL/6 mice. AAV-retro-hSyn-DIO-mCherry-shRNA(TRPC6) (300 nl) or its
684 control AAV-retro-scramble-shRNA was delivered into the mPFC of the DAT-Cre
685 C57BL/6 mice.
686 The shRNA hairpin sequences used in this study:
687 NALCN shRNA: AAGATCGCACAGCCTCTTCAT[29];
688 TRPC6 shRNA: 5'-CCAGGATCAATGCATACAA-3'.
689 For Cre-dependent overexpression of TRPC6, AAV9-DIO-TRPC6-GFP (300 nl) or its
690 control AAV9-scramble-shRNA was delivered into the VTA of the DAT-Cre C57BL/6
691 mice, 7 days after injection of AAV9-hSyn-DIO-shRNA(TRPC6)-RFP.
692 Mice were singly housed with enough food and water to recover for 4-5 weeks after
693 injection of virus, before behavior tests and electrophysiological recordings.
694 **Single cell PCR**
695 mRNA was reversely transcribed to cDNA by PrimeScript^{TM} II 1st Strand cDNA
696 Synthesis Kit (Takara-Clontech, Kyoto, Japan). At the end of electrophysiological
697 recordings, the recorded neuron was aspirated into a pipette and then expelled into a
698 PCR sterile tube containing 1 μl oligo-dT Primer and 1 μl dNTP mixture. The mixture
699 was heated to 65°C for 5 min to denature the nucleic acids and then cooled on ice for
700 2 min. Reverse transcription from mRNA into cDNA was performed at 50°C for 50
701 min and then 85°C for 5 min. cDNA was stored at -40°C. Then two rounds of
702 conventional PCR with pairs of gene-specific outside (first round) and inner primers
703 (second round) for GAPDH (positive control), TH, DAT, D2, GIRK2, VGulT2,
704 GAD1, NALCN, TRPC6, TRPV2, TRPC3, TRPC4 and TRPC7 using GoTaq® Green
705 Master Mix (Promega, Madison, USA) were performed. After adding the specific
706 outside primer pairs into one PCR tube per cell, first-round synthesis conditions were
707 as follows: 95 °C (5 min); 30 cycles of 95 °C (50 s), 58-63 °C (50 s), 72 °C (50 s);
708 72 °C (5 min). Then, the product of the first PCR was added in the second
709 amplification round by using specific inner primer (final volume 25 μl). The second

710 amplification round consisted of the following: 95 °C (5 min); 35 cycles of 95 °C (50
711 s), 58 °C-62 °C (45 s), 72 °C (50 s) and 5 min elongation at 72 °C. The final PCR
712 products were separated by electrophoresis on 2% agarose gels. The negative control
713 reactions with no added cDNA were also performed in each experiment.
714 The "outer" primers (from 5′ to 3′) as follows:
715 GAPDH:
716 AAATGGTGAAGGTCGGTGTGAACG (sense)
717 AGTGATGGCATGGACTGTGGTCAT (antisense)
718 TH:
719 GCCGTCTCAGAGCAGGATAC
720 GGGTAGCATAGAGGCCCTTC
721 DAT:
722 CTGCCCTGTCCTGAAAGGTGT
723 GCCCAGTGATCACAGACTCC
724 D2-R:
725 AGCATCGACAGGTACACAGC
726 CCATTCTCCGCCTGTTCACT
727 GIRK2:
728 TGGACCAGGATGTGGAAAGC
729 AAACCCGTTGAGGTTGGTGA
730 VGluT2:
731 CTGCTTCTGGTTGTTGGCTACTCT
732 ATCTCGGTCCTTATAGGTGTACGC
733 GAD1:
734 ACAACCTTTGGCTGCATGTGGATG
735 AATCCCACGGTGCCCTTTGCTTTC
736 NALCN:
737 TCCATCTGTGGGAAGCATGT
738 CAAAAGCTGGTCCTCTTCAGTG
739 TRPC6:
740 AGCCTGTCTATTGAGGAAGAAC

741 AGCGAGAATGATTGGGGTCA

742 TRPV2:

743 CTGCACATCGCCATAGAGAA

744 AGGCTGGTGGTAGGCAACTA

745 TRPC3:

746 GCTGGCCAACATAGAGAAGG

747 CCTGCACGTGACTATCCACA

748 TRPC4:

749 GTCTATGTAGGCGATGCGCT

750 AGGAGGTCCTTGGCAAATTGT

751 TRPC7:

752 GCCATCAGCAAGGGCTATGT

753 CACGCCCACCACAAAATCC

754 The “inner” primers (from 5′ to 3′) as follows:

755 GAPDH:

756 GCAAATTCAACGGCACAGTCAAGG

757 TCTCGTGGTTCACACCCATCACAA

758 TH:

759 AGGAGAGGGATGGAAATGCT

760 ACCAGGGAACCTTGTCCTCT

761 DAT:

762 ATTTTGAGCGTGGTGTGCTG

763 TGCCTCACAGAGACGGTAGA

764 D2-R:

765 CCATTGTCTGGGTCCTGTCC

766 GTGGGTACAGTTGCCCTTGA

767 GIRK2:

768 AGCCGAGACAGGACCAAAAG

769 ATGTACGCAATCAGCCACCA

770 VGluT2:

771 CATCTCCTTCTTGGTGCTTGCAGT

772 ACAGCGTGCCAACGCCATTTGAAA

773 GAD1:

774 AGTCACCTGGAACCCTC

775 GCTTGTCTGGCTGGAA

776 NALCN:

777 GCCTTTGCTGGAGTTGTTCTG

778 CCCTGCATAATTGCCACAGTC

779 TRPC6:

780 TGCTAGAAGAGTGTCATTCCCT

781 CCTCCACAATCCGTACATAACC

782 TRPV2:

783 GTGGGATGTGGTGACCTACC

784 GCTGGTACAGCCCTGAGAAC

785 TRPC3:

786 CCTTGGGTCTTCCATTCCTC

787 CACAACTGCACGATGTACTCC

788 TRPC4:

789 CCACGAGGTCCGCTGTAAC

790 CTCCCAACTTAACTGAAAGGCA

791 TRPC7:

792 CGCTTCTCCCACGACATCAC

793 ACTGGATAGGGACAGGTAGGC

794 **RT-qPCR**

795 Total RNA was prepared using Trizol. RNA was reversely transcribed into cDNA by

796 TAKARA PrimeScript^{TM} RT reagent Kit with gDNA Eraser for Reverse transcription.

797 Subsequently, the TB Green® Premix Ex Taq™ II (Tli RNaseH Plus) (TaKaRa) was

798 used to do the RT-qPCR assays.

799 The specific primers were:

800 GAPDH：

801 GCAAATTCAACGGCACAGTCAAGG

802 TCTCGTGGTTCACACCCATCACAA

803 TRPC6：
804 GCAGAAACACAGAGGAAGTGG
805 GCTCTTTCCAGCTTGGCATATC
806 NALCN：
807 TAATGAGATAGGCACGAGTA
808 TGATGAAGTAGAAGTAGGAG
809
810 **Single cell RT-qPCR**
811 Following the retrograde labelling and VTA brain slice preparation,
812 projection-specific VTA neurons were identified by infrared-differential interference
813 contrast (IR-DIC) video microscopy and epifluorescence (Olympus, Japan) for
814 detection of retrobeads (red) positive neurons. mRNA was reversely transcribed to
815 cDNA by PrimeScript^{TM} II 1st Strand cDNA Synthesis Kit (Takara-Clontech, Kyoto,
816 Japan). The projection-specific neuron was aspirated into a pipette and then expelled
817 into a PCR sterile tube containing 1 μl oligo-dT Primer and 1 μl dNTP mixture. The
818 mixture was heated to 65°C for 5 min to denature the nucleic acids and then cooled on
819 ice for 2 min. Reverse transcription from mRNA into cDNA was performed at 50°C
820 for 50 min and then 85°C for 5 min. cDNA was stored at -40°C. The targeted
821 pre-amplification was done, with pairs of targeted primers for GAPDH, TH and
822 TRPC6, to quantify multiple targets per cell. After adding the targeted primer pairs
823 into each PCR tube, the synthesis conditions were as follows: 95 °C (5 min); 10
824 cycles of 95 °C (50 s), 58-62 °C (50 s), 72 °C (50 s); 72 °C (5 min). After targeted
825 pre-amplification, quantitative PCR (qPCR) is the final laboratory step of the
826 scRT-qPCR workflow with the TB Green® Premix Ex Taq™ II (Tli RNaseH Plus)
827 (TaKaRa).
828 The targeted primers for pre-amplification (from 5′to 3′) as follows:
829 GAPDH:
830 AAATGGTGAAGGTCGGTGTGAACG (sense)
831 AGTGATGGCATGGACTGTGGTCAT (antisense)
832 TH:
833 AAGGTTCATTGGACGGCGG

834 ACATCGTCAGACACCCGAC
835 TRPC6:
836 AGCCTGTCTATTGAGGAAGAAC
837 AGCGAGAATGATTGGGGTCA
838 The primers for qPCR (from 5′ to 3′) as follows:
839 GAPDH:
840 GCAAATTCAACGGCACAGTCAAGG
841 TCTCGTGGTTCACACCCATCACAA
842 TH:
843 TCTCCTTGAGGGGTACAAAACC
844 ACCTCGAAGCGCACAAAGT
845 TRPC6:
846 TGCTAGAAGAGTGTCATTCCCT
847 CCTCCACAATCCGTACATAACC
848
849 **Immunofluorescence**
850 After intracardial perfusion with 4% paraformaldehyde (PFA) in 0.01 M PBS (pH 7.4),
851 the brains were post-fixed in 4% paraformaldehyde. 48 h later, the brain tissue was
852 placed in 30% sucrose solution (PBS preparation) to dehydrate. The brain tissue was
853 sectioned coronally, including the nucleus accumbens (NAc), medial prefrontal cortex
854 (mPFC), basolateral amygdala (BLA), and VTA, using a vibrating microtome. The
855 section thickness of NAc, mPFC and BLA was 80μm and the section thickness of
856 VTA was 40 μm. The sections were placed in PBS solution and stored in a
857 refrigerator at 4°C for storage.
858 The brain section was incubated in 0.3% triton/3% BSA for 1 h at room temperature
859 and then was blocked with 10% donkey serum at 37°C for 1 h. After that, the brain
860 section was incubated in the corresponding antibodies in PBS at 4°C for 24 h. The
861 section was washed three times (10 min) with PBS. Finally, the brain section was
862 incubated in the secondary antibodies for 2 h at 37°C. Images were obtained on a
863 Leica TCS SP5 confocal laser microscope (Leica, Germany) equipped with laser lines
864 for 405 mm, 488 mm, 561 mm and 647 mm illumination. Images were analyzed with

865 LAS-AF-Lite software (Leica, Germany).

866

867 **Single-cell whole-transcriptome gene sequencing**

868 After retrobeads injection, following brain slice preparation and recording, the
869 recorded and retrobeads-labelled neurons were aspirated into the patch pipette and
870 were then broken into the PCR tube containing 1 μl lysis buffer. For mRNA in
871 individual cells, mRNA was amplified and cDNA by SMARTer Ultra Low Input RNA
872 for Illumina Kit, which was qualified and reversely transcribed to cDNA by Qubit and
873 Agilent Bioanalyzer 2100 electrophoresis. After fragmentation of cDNA (300 bp) by
874 ultrasound, sequencing libraries (end repair, addition of poly(A), and ligation of
875 sequencing connectors) were built using the Ovation Ultralow Library System V2.
876 After that, the constructed libraries were sequenced using Illumina HiseqXten.

877

878 **Depression models**

879 Chronic Mild Unpredictable Stress (CMUS) procedure

880 The CMUS procedures consisted of food and water deprivation (24 h), day/night
881 inversion, damp bedding (12 h), cage tilt (12 h), no bedding (12 h), rat bedding (12 h),
882 4°C cold bath (5 min), restraint (2 h) and tail pinching (30 min). Mice were subjected
883 to consecutive 35 days of CMUS with two stressors per day. Non-stressed controls
884 were handled only for cage changes and behavioral tests.

885 Chronic Restraint Stress (CRS) procedure

886 The mice were immobilized in a special restraint device for 6 h per day from 9:00 to
887 15:00 for 21 days.

888 Behavior tests

889 The behavior tests were performed in the following order.

890 Sucrose preference test

891 Mice were single-housed and trained to drink from two drinking bottles with 1 bottle
892 of tap water and 1 bottle of 1.0 % sucrose water, for 48 hours, and the positions of the
893 drinking bottles were exchanged every 12 h to exclude the interference of position
894 preference. After the training, the mice were deprived of food and water for 12 h, and
895 then the sucrose preference test was performed for 24 h. One bottle of tap water and

one bottle of 1.0 % sucrose water were given again, and the positions of the drinking bottles were exchanged at 12 h. Finally, the consumption of tap water and sugar water at 24 h were recorded to calculate the sucrose solution preference rate. Sucrose preference rate (%) = sucrose solution consumption/(tap water consumption + sucrose solution consumption)*100%.

Open field test, OFT

The mice were placed in a topless chamber (40 cm × 40 cm × 30 cm) with a camera mounted on top of the chamber and connected to ANY-maze video tracking system on the computer to automatically track and record the activity of mice during the experiment and to obtain behavioral data. The bottom of the chamber was divided into 16 small square grids (10 cm × 10 cm) on the computer, and four square grids in the central area were defined as the central zone. During the 10 min test session, total distance traveled and time spent in the center were recorded.

Elevated plus maze, EPM

The EPM apparatus consists of two closed arms (25 × 5 cm) across from each other and perpendicular to two open arms (25 × 5 cm) that are connected by a center platform (5 × 5 cm), with a camera in the center ceiling to automatically track and record the activity of mice. Mice were placed in the center platform facing a closed arm and allowed to freely explore the maze for 7 min, of which the first 2 min was the adaptation time. The time spent in open and closed arms was analyzed for last 5 min after the adaptation.

Accelerating rotarod test

Locomotor activity was estimated by accelerating the rotarod test. Each group of animals was placed on an accelerating rotarod walking for 300 s from 4 to 40 rpm. After three days of training (three times per day), latency was recorded from the beginning of the trial until the mouse falls off for 300 s from 4 to 40 rpm.

Forced swimming test, FST

Forced swimming test (FST) was performed in a glass cylinder, filled with the water depth about 15 cm at room temperature. The experiment was conducted for 5 min, of which the first 1 min was the adaptation time and the mice were allowed to move freely, and the immobility time was recorded for last 4 min after the adaptation.

927 Tail suspension test, TST

928 Mouse was suspended by taping the tail (1 cm from the tip of the tail) to the fixation
929 device for 6 min. The cumulative immobility time within last 4 min was recorded, and
930 the time when all limbs were immobile except for respiration was considered as
931 immobility time.

932

933 **Western Blot**

934 VTA was carefully obtained from the coronal midbrain slices (900 μm-thick) with a
935 small homemade biopsy punch (1.0 mm in diameter) on ice, which was verified using
936 the Franklin and Paxinos mouse brain atlas[77], and then stored at -80 °C until the day
937 of the experiment. The VTA protein was isolated by100 μl RIPA and 1 μl PMSF. The
938 total protein for each sample was transferred onto the polyvinylidene difluoride
939 (PVDF) membranes after SDS-polyacrylamide gel electrophoresis (SDS-PAGE), and
940 blocked 2 h at room temperature with 5% bovine serum albumin (KeyGen
941 Biotechnology). Subsequently, all these membranes were incubated overnight at 4 °C
942 with the primary antibodies as below: TRPC6, NALCN, and GAPDH. Following 2 h
943 secondary antibodies incubation, all the bands were detected. The relative expression
944 was calculated based on the internal control GAPDH.

945

946 **Drugs and reagents**

947 Drugs were bath applied at the following
948 concentrations:6-cyano-7-nitroquinoxaline-2,3-dione (CNQX; 10 μM; Sigma),
949 DL-2-amino-5-phosphonopentanoic acid (APV; 50 μM; Sigma) and gabazine (10 μM;
950 Sigma), CsCl (3mM; sigma), ZD7288 (60 μm; Abcam), TTX (1 μM; MCE and
951 CHENGDU MUST BIO-TECHNOLOGY CO., LTD), $GdCl_3$ (100 μM; Sigma),
952 L703,606 (10 μM; Sigma), 2-Aminoethyldiphenylborinate (2-APB, 100 μM; Sigma),
953 Larixyl acetate (10 μM; Sigma), Ruthenium Red (60 μM; TCI).

954 Commercial antibodies used were: Anti-Tyrosine Hydroxylase Antibody (1:400,
955 Millipore, MAB318, RRID: AB_2201528, for Immunofluorescence), Anti-Dopamine
956 Transporter (N-terminal) antibody (1:400, sigma, D6944, RRID: AB_1840807, for
957 Immunofluorescence), Anti-NALCN (1:100, Thermo Fisher Scientific, MA5-27593,
958 RRID: AB_2735285, for Immunofluorescence), Anti-TRPC6 (1:100, Alomone,

959 ACC-017, RRID: AB_2040243, for Immunofluorescence), Anti-GAPDH (1:10000,
960 Santa Cruz, sc-137179, RRID: AB_2232048, for Western Blot), Anti-NALCN (1:100,
961 GeneTex, GTX54808, RRID: AB_3097701, for Western Blot), Anti-TRPC6 (1:100,
962 Cell Signaling Technology, 16716, RRID: AB_2798768, for Western Blot).
963 Secondary antibodies: Donkey anti-Mouse IgG (H+L) Highly Cross-Adsorbed
964 Secondary Antibody (Alexa Fluor 488, Thermo Fisher Scientific, A-21202, 1:1000),
965 Donkey anti-Mouse IgG (H+L) Highly Cross-Adsorbed Secondary Antibody (Alexa
966 Fluor 546, Thermo Fisher Scientific, A10037, 1:1000), Donkey anti-Rabbit IgG (H+L)
967 Highly Cross-Adsorbed Secondary Antibody (Alexa Fluor 488, Thermo Fisher
968 Scientific, A21206, 1:1000), Donkey anti- Rabbit IgG (H+L) Highly Cross-Adsorbed
969 Secondary Antibody (Alexa Fluor 546, Thermo Fisher Scientific, A10040, 1:1000),
970 Donkey anti-Rabbit IgG (H+L) Highly Cross-Adsorbed Secondary Antibody (Alexa
971 Fluor 647, Thermo Fisher Scientific, A31573, 1:1000)
972
973 **Quantification and statistical analysis**
974 Software such as GraphPad Prism6, OriginPro 8.0 (Origin Lab) and Adobe Illustrator
975 CS6 were used for data analysis and image processing. All experimental data were
976 expressed as mean ± standard error (mean ± S.E.M.). When the data were normally
977 distributed, the difference between two groups was statistically analyzed by
978 two-sample T-test or paired-sample T-test; when the data were not normally
979 distributed, the difference between two groups was statistically analyzed by
980 Mann-Whitney U test or Wilcoxon matched-pairs signed rank test. $P < 0.05$ was
981 considered as a statistically significant difference between two groups. For the data
982 between multiple groups, when the data were normally distributed and there was no
983 significant variance inhomogeneity, one-way ANOVA with Dunnett's multiple
984 comparisons test or two-way ANOVA with Sidak's multiple comparisons test was
985 used; when the data were not normally distributed, Kruslal-Wallis-H test with
986 Dunnett's multiple comparisons test was used.
987 **Conflict of Interest**
988 The authors declare that the research was conducted in the absence of any commercial
989 or financial relationships that could be construed as a potential conflict of interest.
990 **Author Contributions**

Hailin Zhang conceived, designed and supervised the experiments; Jing Wang performed the experiments, acquired and analyzed the data and prepared the figures; Dongmei Zhang and Min Su performed immunofluorescence of the brain slices and performed some preliminary electrophysiological experiments; Yuqi Sang and Chaoyi Li performed part of single-cell PCR; Yongxue Zhang performed partof statistical analysis; Ludi Zhang and Chenxu Niu took care of mice; Hailin Zhang and Jing Wang wrote the manuscript; Hailin Zhang and Xiaona Du prepared the final version of the manuscript.

Funding

This work was supported by the National Natural Science Foundation of China (81871075, 82071533) grants to HZ; National Natural Science Foundation of China (81870872, U21A20359) grants to XD; Science Fund for Creative Research Groups of Natural Science Foundation of Hebei Province (no. H2020206474); Basic Research Fund for Provincial Universities (JCYJ2021010), Natural Science Foundation of Hebei Province (H2023423065)，Science and Technology Research Project of Higher Education Institutions in Hebei Province (QN2024159) and Scientific Research Project of Hebei Administration of Traditional Chinese Medicine (2024091) grants to WJ.

Acknowledgments

We would like to thank colleagues at the Core Facilities and Centers of Hebei Medical University for the technical assistance.

Data Availability Statement

The data that support the findings of this study are available from the corresponding author upon reasonable request.

References

1. Bromberg-Martin, E.S., M. Matsumoto, and O. Hikosaka, *Dopamine in motivational control: rewarding, aversive, and alerting.* Neuron, 2010. **68**(5): p. 815-34.
2. Lammel, S., B.K. Lim, and R.C. Malenka, *Reward and aversion in a heterogeneous midbrain dopamine system.* Neuropharmacology, 2014. **76 Pt B**(0 0): p. 351-9.
3. Van den Heuvel, D.M. and R.J. Pasterkamp, *Getting connected in the dopamine system.* Prog Neurobiol, 2008. **85**(1): p. 75-93.
4. Chaudhury, D., et al., *Rapid regulation of depression-related behaviours by control of midbrain dopamine neurons.* Nature, 2013. **493**(7433): p. 532-6.

1024 5. Kabanova, A., et al., *Function and developmental origin of a mesocortical inhibitory circuit.*
1025 Nat Neurosci, 2015. **18**(6): p. 872-82.
1026 6. Badrinarayan, A., et al., *Aversive stimuli differentially modulate real-time dopamine*
1027 *transmission dynamics within the nucleus accumbens core and shell.* J Neurosci, 2012. **32**(45):
1028 p. 15779-90.
1029 7. Friedman, A.K., et al., *Enhancing depression mechanisms in midbrain dopamine neurons*
1030 *achieves homeostatic resilience.* Science, 2014. **344**(6181): p. 313-9.
1031 8. Krishnan, V., et al., *Molecular adaptations underlying susceptibility and resistance to social*
1032 *defeat in brain reward regions.* Cell, 2007. **131**(2): p. 391-404.
1033 9. Grace, A.A., et al., *Regulation of firing of dopaminergic neurons and control of goal-directed*
1034 *behaviors.* Trends Neurosci, 2007. **30**(5): p. 220-7.
1035 10. Johnson, S.W. and R.A. North, *Two types of neurone in the rat ventral tegmental area and*
1036 *their synaptic inputs.* J Physiol, 1992. **450**: p. 455-68.
1037 11. Zhong, P., et al., *HCN2 channels in the ventral tegmental area regulate behavioral responses*
1038 *to chronic stress.* Elife, 2018. **7**.
1039 12. Bean, B.P., *The action potential in mammalian central neurons.* Nat Rev Neurosci, 2007. **8**(6):
1040 p. 451-65.
1041 13. Guzman, J.N., et al., *Robust pacemaking in substantia nigra dopaminergic neurons.* J Neurosci,
1042 2009. **29**(35): p. 11011-9.
1043 14. Puopolo, M., E. Raviola, and B.P. Bean, *Roles of subthreshold calcium current and sodium*
1044 *current in spontaneous firing of mouse midbrain dopamine neurons.* J Neurosci, 2007. **27**(3):
1045 p. 645-56.
1046 15. Khaliq, Z.M. and B.P. Bean, *Pacemaking in dopaminergic ventral tegmental area neurons:*
1047 *depolarizing drive from background and voltage-dependent sodium conductances.* J Neurosci,
1048 2010. **30**(21): p. 7401-13.
1049 16. Beckstead, M.J., et al., *Vesicular dopamine release elicits an inhibitory postsynaptic current in*
1050 *midbrain dopamine neurons.* Neuron, 2004. **42**(6): p. 939-46.
1051 17. Ford, C.P., M.J. Beckstead, and J.T. Williams, *Kappa opioid inhibition of somatodendritic*
1052 *dopamine inhibitory postsynaptic currents.* J Neurophysiol, 2007. **97**(1): p. 883-91.
1053 18. Philippart, F., et al., *Differential Somatic Ca2+ Channel Profile in Midbrain Dopaminergic*
1054 *Neurons.* J Neurosci, 2016. **36**(27): p. 7234-45.
1055 19. Dufour, M.A., A. Woodhouse, and J.M. Goaillard, *Somatodendritic ion channel expression in*
1056 *substantia nigra pars compacta dopaminergic neurons across postnatal development.* J
1057 Neurosci Res, 2014. **92**(8): p. 981-99.
1058 20. Kimm, T., Z.M. Khaliq, and B.P. Bean, *Differential Regulation of Action Potential Shape and*
1059 *Burst-Frequency Firing by BK and Kv2 Channels in Substantia Nigra Dopaminergic Neurons.* J
1060 Neurosci, 2015. **35**(50): p. 16404-17.
1061 21. Li, L., et al., *Selective targeting of M-type potassium K(v) 7.4 channels demonstrates their key*
1062 *role in the regulation of dopaminergic neuronal excitability and depression-like behaviour.* Br J
1063 Pharmacol, 2017. **174**(23): p. 4277-4294.
1064 22. Tarfa, R.A., R.C. Evans, and Z.M. Khaliq, *Enhanced Sensitivity to Hyperpolarizing Inhibition in*
1065 *Mesoaccumbal Relative to Nigrostriatal Dopamine Neuron Subpopulations.* J Neurosci, 2017.
1066 **37**(12): p. 3311-3330.
1067 23. Seutin, V., et al., *Evidence for a modulatory role of Ih on the firing of a subgroup of midbrain*

1068 *dopamine neurons.* Neuroreport, 2001. **12**(2): p. 255-8.
1069 24. Neuhoff, H., et al., *I(h) channels contribute to the different functional properties of identified*
1070 *dopaminergic subpopulations in the midbrain.* J Neurosci, 2002. **22**(4): p. 1290-302.
1071 25. Krashia, P., et al., *On the properties of identified dopaminergic neurons in the mouse*
1072 *substantia nigra and ventral tegmental area.* Eur J Neurosci, 2017. **45**(1): p. 92-105.
1073 26. Chua, H.C., et al., *The NALCN channel complex is voltage sensitive and directly modulated by*
1074 *extracellular calcium.* Sci Adv, 2020. **6**(17): p. eaaz3154.
1075 27. Lu, B., et al., *Peptide neurotransmitters activate a cation channel complex of NALCN and*
1076 *UNC-80.* Nature, 2009. **457**(7230): p. 741-4.
1077 28. Philippart, F. and Z.M. Khaliq, *G(i/o) protein-coupled receptors in dopamine neurons inhibit*
1078 *the sodium leak channel NALCN.* Elife, 2018. **7**.
1079 29. Shi, Y., et al., *Nalcn Is a "Leak" Sodium Channel That Regulates Excitability of Brainstem*
1080 *Chemosensory Neurons and Breathing.* J Neurosci, 2016. **36**(31): p. 8174-87.
1081 30. Lutas, A., et al., *The leak channel NALCN controls tonic firing and glycolytic sensitivity of*
1082 *substantia nigra pars reticulata neurons.* Elife, 2016. **5**.
1083 31. Ford, N.C., D. Ren, and M.L. Baccei, *NALCN channels enhance the intrinsic excitability of spinal*
1084 *projection neurons.* Pain, 2018. **159**(9): p. 1719-1730.
1085 32. Um, K.B., et al., *TRPC3 and NALCN channels drive pacemaking in substantia nigra*
1086 *dopaminergic neurons.* Elife, 2021. **10**.
1087 33. Kim, S.H., et al., *Nonselective cation channels are essential for maintaining intracellular Ca2+*
1088 *levels and spontaneous firing activity in the midbrain dopamine neurons.* Pflugers Arch, 2007.
1089 **455**(2): p. 309-21.
1090 34. Zhou, F.W., S.G. Matta, and F.M. Zhou, *Constitutively active TRPC3 channels regulate basal*
1091 *ganglia output neurons.* J Neurosci, 2008. **28**(2): p. 473-82.
1092 35. Hof, T., et al., *Transient receptor potential channels in cardiac health and disease.* Nat Rev
1093 Cardiol, 2019. **16**(6): p. 344-360.
1094 36. Klipec, W.D., et al., *Loss of the trpc4 gene is associated with a reduction in cocaine*
1095 *self-administration and reduced spontaneous ventral tegmental area dopamine neuronal*
1096 *activity, without deficits in learning for natural rewards.* Behav Brain Res, 2016. **306**: p.
1097 117-27.
1098 37. German, D.C. and K.F. Manaye, *Midbrain dopaminergic neurons (nuclei A8, A9, and A10):*
1099 *three-dimensional reconstruction in the rat.* J Comp Neurol, 1993. **331**(3): p. 297-309.
1100 38. Nair-Roberts, R.G., et al., *Stereological estimates of dopaminergic, GABAergic and*
1101 *glutamatergic neurons in the ventral tegmental area, substantia nigra and retrorubral field in*
1102 *the rat.* Neuroscience, 2008. **152**(4): p. 1024-31.
1103 39. Cadwell, C.R., et al., *Electrophysiological, transcriptomic and morphologic profiling of single*
1104 *neurons using Patch-seq.* Nat Biotechnol, 2016. **34**(2): p. 199-203.
1105 40. Lammel, S., et al., *Unique properties of mesoprefrontal neurons within a dual*
1106 *mesocorticolimbic dopamine system.* Neuron, 2008. **57**(5): p. 760-73.
1107 41. Kawano, M., et al., *Particular subpopulations of midbrain and hypothalamic dopamine*
1108 *neurons express vesicular glutamate transporter 2 in the rat brain.* J Comp Neurol, 2006.
1109 **498**(5): p. 581-92.
1110 42. Patel, J.C., et al., *GABA co-released from striatal dopamine axons dampens phasic dopamine*
1111 *release through autoregulatory GABA(A) receptors.* Cell Rep, 2024. **43**(3): p. 113834.

1112 43. Tritsch, N.X., A.J. Granger, and B.L. Sabatini, *Mechanisms and functions of GABA co-release.*
1113 Nat Rev Neurosci, 2016. **17**(3): p. 139-45.
1114 44. Lu, B., et al., *The neuronal channel NALCN contributes resting sodium permeability and is*
1115 *required for normal respiratory rhythm.* Cell, 2007. **129**(2): p. 371-83.
1116 45. Kusch, J., et al., *Interdependence of receptor activation and ligand binding in HCN2*
1117 *pacemaker channels.* Neuron, 2010. **67**(1): p. 75-85.
1118 46. Mistrík, P., et al., *The murine HCN3 gene encodes a hyperpolarization-activated cation*
1119 *channel with slow kinetics and unique response to cyclic nucleotides.* J Biol Chem, 2005.
1120 **280**(29): p. 27056-61.
1121 47. Clapham, D.E., L.W. Runnels, and C. Strübing, *The TRP ion channel family.* Nat Rev Neurosci,
1122 2001. **2**(6): p. 387-96.
1123 48. Urban, N., et al., *Identification and Validation of Larixyl Acetate as a Potent TRPC6 Inhibitor.*
1124 Mol Pharmacol, 2016. **89**(1): p. 197-213.
1125 49. Strübing, C., et al., *Formation of novel TRPC channels by complex subunit interactions in*
1126 *embryonic brain.* J Biol Chem, 2003. **278**(40): p. 39014-9.
1127 50. Goel, M., W.G. Sinkins, and W.P. Schilling, *Selective association of TRPC channel subunits in rat*
1128 *brain synaptosomes.* J Biol Chem, 2002. **277**(50): p. 48303-10.
1129 51. Tye, K.M., et al., *Dopamine neurons modulate neural encoding and expression of*
1130 *depression-related behaviour.* Nature, 2013. **493**(7433): p. 537-541.
1131 52. Chang, C.H. and A.A. Grace, *Amygdala-ventral pallidum pathway decreases dopamine activity*
1132 *after chronic mild stress in rats.* Biol Psychiatry, 2014. **76**(3): p. 223-30.
1133 53. Moreines, J.L., Z.L. Owrutsky, and A.A. Grace, *Involvement of Infralimbic Prefrontal Cortex but*
1134 *not Lateral Habenula in Dopamine Attenuation After Chronic Mild Stress.*
1135 Neuropsychopharmacology, 2017. **42**(4): p. 904-913.
1136 54. Willner, P., *The chronic mild stress (CMS) model of depression: History, evaluation and usage.*
1137 Neurobiol Stress, 2017. **6**: p. 78-93.
1138 55. Liu, D., et al., *Brain-derived neurotrophic factor-mediated projection-specific regulation of*
1139 *depressive-like and nociceptive behaviors in the mesolimbic reward circuitry.* Pain, 2018.
1140 **159**(1): p. 175.
1141 56. Kang, Y. and S.T. Kitai, *A whole cell patch-clamp study on the pacemaker potential in*
1142 *dopaminergic neurons of rat substantia nigra compacta.* Neurosci Res, 1993. **18**(3): p. 209-21.
1143 57. Lu, B., et al., *Extracellular calcium controls background current and neuronal excitability via*
1144 *an UNC79-UNC80-NALCN cation channel complex.* Neuron, 2010. **68**(3): p. 488-99.
1145 58. Benarroch, E.E., *HCN channels: function and clinical implications.* Neurology, 2013. **80**(3): p.
1146 304-10.
1147 59. Mercuri, N.B., et al., *Properties of the hyperpolarization-activated cation current Ih in rat*
1148 *midbrain dopaminergic neurons.* Eur J Neurosci, 1995. **7**(3): p. 462-9.
1149 60. Okamoto, T., M.T. Harnett, and H. Morikawa, *Hyperpolarization-activated cation current (Ih) is*
1150 *an ethanol target in midbrain dopamine neurons of mice.* J Neurophysiol, 2006. **95**(2): p.
1151 619-26.
1152 61. Chan, C.S., et al., *'Rejuvenation' protects neurons in mouse models of Parkinson's disease.*
1153 Nature, 2007. **447**(7148): p. 1081-6.
1154 62. Lee, J.H., L.L. Cribbs, and E. Perez-Reyes, *Cloning of a novel four repeat protein related to*
1155 *voltage-gated sodium and calcium channels.* FEBS Lett, 1999. **445**(2-3): p. 231-6.

63. Lu, T.Z. and Z.P. Feng, *NALCN: a regulator of pacemaker activity.* Mol Neurobiol, 2012. **45**(3): p. 415-23.
64. Pochwat, B., et al., *Hyperforin Potentiates Antidepressant-Like Activity of Lanicemine in Mice.* Front Mol Neurosci, 2018. **11**: p. 456.
65. Liu, Y., et al., *The change of spatial cognition ability in depression rat model and the possible association with down-regulated protein expression of TRPC6.* Behav Brain Res, 2015. **294**: p. 186-93.
66. Cao, J.L., et al., *Mesolimbic dopamine neurons in the brain reward circuit mediate susceptibility to social defeat and antidepressant action.* J Neurosci, 2010. **30**(49): p. 16453-8.
67. Eder, P., et al., *Na(+) entry and modulation of Na(+)/Ca(2+) exchange as a key mechanism of TRPC signaling.* Pflugers Arch, 2005. **451**(1): p. 99-104.
68. Hahn, S., et al., *Proximal dendritic localization of NALCN channels underlies tonic and burst firing in nigral dopaminergic neurons.* J Physiol, 2023. **601**(1): p. 171-193.
69. Inoue, R. and Y. Mori, *Molecular candidates for capacitative and non-capacitative Ca2+ entry in smooth muscle.* Novartis Found Symp, 2002. **246**: p. 81-90; discussion 221-7.
70. Nishida, M., et al., *Phosphorylation of TRPC6 channels at Thr69 is required for anti-hypertrophic effects of phosphodiesterase 5 inhibition.* J Biol Chem, 2010. **285**(17): p. 13244-53.
71. Nishioka, K., et al., *Cilostazol suppresses angiotensin II-induced vasoconstriction via protein kinase A-mediated phosphorylation of the transient receptor potential canonical 6 channel.* Arterioscler Thromb Vasc Biol, 2011. **31**(10): p. 2278-86.
72. Su, M., et al., *Kv7.4 Channel Contribute to Projection-Specific Auto-Inhibition of Dopamine Neurons in the Ventral Tegmental Area.* Front Cell Neurosci, 2019. **13**: p. 557.
73. McCall, N.M., E. Marron Fernandez de Velasco, and K. Wickman, *GIRK Channel Activity in Dopamine Neurons of the Ventral Tegmental Area Bidirectionally Regulates Behavioral Sensitivity to Cocaine.* J Neurosci, 2019. **39**(19): p. 3600-3610.
74. Qu, N., et al., *A POMC-originated circuit regulates stress-induced hypophagia, depression, and anhedonia.* Mol Psychiatry, 2020. **25**(5): p. 1006-1021.
75. Butterweck, V., *Mechanism of action of St John's wort in depression : what is known?* CNS Drugs, 2003. **17**(8): p. 539-62.
76. Burlet, S., C.J. Tyler, and C.S. Leonard, *Direct and indirect excitation of laterodorsal tegmental neurons by Hypocretin/Orexin peptides: implications for wakefulness and narcolepsy.* J Neurosci, 2002. **22**(7): p. 2862-72.
77. Jan-Pieter and Konsman, *The mouse brain in stereotaxic coordinates: Second Edition (Deluxe) By Paxinos G. and Franklin, K.B.J., Academic Press, New York, 2001, ISBN 0-12-547637-X.* Psychoneuroendocrinology, 2003.

1194 **Figure legends**

1195 **Fig.1** The effects of extracellular Ca^{2+} and Na^{+} on firing activity of the male and
1196 female VTA DA neurons.

1197 **A**. Identification of the VTA DA neurons. i: confocal images showing the anatomical
1198 distribution of DA neurons in the VTA and SNc; the DA neurons were identified to be
1199 DAT-immunofluorescence positive (scale bar, 100 μm). ii: left panel: single-cell PCR
1200 results; four cells (C1-C4) showed the presence of genes indicated. right panel:
1201 Percentage of neuronal markers (DA neuron: TH, DAT, D_2R, Girk2; Glu neuron:
1202 VGluT2 and GABA neuron: GAD1) positive neurons in the VTA neurons (GAPDH
1203 positive). n = 102 cells, N = 22. **B**. The effect of replacing extracellular Ca^{2+} with
1204 Mg^{2+} on firing frequency of the male and female VTA DA neurons. Example
1205 time-course (i) and traces (ii) of the spontaneous firing before and after replacement
1206 of extracellular Ca^{2+} (2 mM) by an equimolar amount of Mg^{2+}.The inset on the top of
1207 ii shows a map of a coronal midbrain slice indicating the location of neurons that were
1208 recorded and subsequently identified as DA neurons which were DAT positive with
1209 single cell-PCR (red dots). iii: Summarized data for ii. Firing of the VTA DA neurons
1210 were recorded using loose cell-attached patch from a brain slice of the VTA (n = 32, N
1211 = 16). Wilcoxon matched-pairs signed rank test, W = 526.0, ****$P < 0.0001$. **C**. The
1212 effect of replacing extracellular Ca^{2+} with Mg^{2+} on the resting membrane potential
1213 (RMP) of the male and female VTA DA neurons, in the presence of 1 μM TTX.
1214 Example time-course (i) and summarized data (ii) for the resting membrane potential
1215 before and after replacement of extracellular Ca^{2+} (2 mM) by an equimolar amount of
1216 Mg^{2+} (n = 25, N = 15). The inset on the top of ii shows a map of a coronal midbrain
1217 slice indicating the location of neurons that were recorded and subsequently identified
1218 as DA neurons which were DAT positive with single cell-PCR (red dots).
1219 Paired-sample T test, t = 2.368, df = 24, 95% CI: 0.1454 to 2.119, *$P = 0.0263$. **D.**
1220 Replacement of external Na^{+} by equimolar NMDG resulted in hyperpolarization of
1221 the resting membrane potential of the male and female VTA DA neurons, in the
1222 presence of 1 μM TTX. Example time-course (i) and summarized data (ii) for the
1223 resting membrane potential before and after replacement of extracellular Na^{+} (151
1224 mM) with an equimolar amount of NMDG (n = 17, N = 10). The inset on the top of ii
1225 shows a map of a coronal midbrain slice indicating the location of neurons that were
1226 recorded and subsequently identified as DA neurons which were DAT positive with

1227 single cell-PCR (red dots). Paired-sample T test, t = 7.103, df = 16, 95% CI: -15.35 to
1228 -8.293, ****P < 0.0001. * P < 0.05, **** P < 0.0001. n is number of neurons
1229 recorded and N is number of mice used.
1230
1231 **Fig. 2** Gene expression profile of non-selective cation channels (NSCCs) in the male
1232 VTA DA neurons.
1233 Single-cell RNA-Seq was performed on the VTA neurons projecting to five different
1234 brain regions of male mice (NAc c, NAc ms, NAc ls, BLA, mPFC). **A**. Gene
1235 expression profile of markers for neuron subtypes from 45 VTA neurons; the neuron
1236 subtypes included: dopaminergic (Th, Ddc, DAT), GABAergic (Gad1, Gad2, VGAT)
1237 and glutamatergic (VGluT2, VGluT1, VGluT3), which was arranged in different rows
1238 indicated in the right labels and in the left-colored vertical lines; projection targets of
1239 these neurons were indicated at the top by the colored lines and labels. Relative
1240 expression levels of these genes were indicated by the dark-blue color intensity which
1241 was transformed from the log2 values of the number of transcripts per million (FPKM)
1242 plus 1. **B**. Relative gene expression levels of TRP channels (i) and other NSCCs (ii) in
1243 45 individual VTA DA neurons and the population average (mean, right columns).
1244 Each column of the individual neurons in (i) and (ii) corresponded to the columns in
1245 A. (iii) Bar graph of the mean log2 (FPKM +1) for the top 8 NSCCs in descending
1246 order. Error bars indicate SEM. **C.** Gene expression profile of aforementioned top 8
1247 NSCCs from 45 VTA neurons.
1248
1249 **Fig. 3** NALCN contributes to subthreshold depolarization and spontaneous firing of
1250 the VTA DA neurons.
1251 **A**. Confocal images showing co-expression of NALCN (green) and DAT (red)
1252 representing DA neurons (scale bar, 10 μm). **B**. i: Single-cell PCR from the VTA DA
1253 neurons (C1-C5) with the expression of NALCN. ii: Percentage of NALCN positive
1254 neurons from 15 DA neurons (with expression of DAT). **C**. Example time-course (i)
1255 and summarized data (ii) showed that NALCN channel blocker ($GdCl_3$) significantly
1256 hyperpolarized the resting membrane potential (RMP) (n = 7, N = 7) of male VTA DA
1257 neurons. The inset on the top of Cii shows a map of a coronal midbrain slice
1258 indicating the location of neurons that were recorded and subsequently identified as
1259 DA neurons which were DAT positive with single cell-PCR (red dots). Paired-sample

T test, t = 11.38, df = 6, 95% CI: -24.30 to -15.70, ****P < 0.0001. **D**. Example time-course and traces (i) and summarized data (ii) of the effect of $GdCl_3$ on spontaneous firing frequency in male VTA DA neurons (n = 7, N = 3). The inset on the top of Dii shows a map of a coronal midbrain slice indicating the location of neurons that were recorded and subsequently identified as DA neurons which were DAT positive with single cell-PCR (red dots). Paired-sample T test, t = 5.711, df = 6, 95% CI: -0.8183 to -0.3274, **P = 0.0012. **E**. Example time-course (i) and summarized data (ii) showed that NALCN channel blocker (L703,606) significantly hyperpolarized the resting membrane potential (RMP) (n = 6, N = 4) of VTA DA neurons in male mice. The inset on the top of Eii shows a map of a coronal midbrain slice indicating the location of neurons that were recorded and subsequently identified as DA neurons which were DAT positive with single cell-PCR (red dots). Paired-sample T test, t = 14.95, df = 5, 95% CI: -5.498 to -3.885, ****P < 0.0001. **F**. Example time-course and traces (i) and summarized data (ii) of the effect of L703,606 on spontaneous firing frequency in DA neurons of both sexes (n = 20, N = 10). The inset on the top of Fii shows a map of a coronal midbrain slice indicating the location of neurons that were recorded and subsequently identified as DA neurons which were DAT positive with single cell-PCR (red dots). Wilcoxon matched-pairs signed rank test, W = -210.0, ****P < 0.0001.**G**. shRNA against NALCN carried by AAV virus (i) (NALCN-shRNA) was injected into the VTA of mice, the mRNA level in the shRNA-NALCN transfected VTA (NALCN-KD, N = 6) and the scramble shRNA transfected VTA (Control, N = 6) was analyzed using qPCR (ii). Two-sample T test, t = 3.714, df = 10, 95% CI: -1.200 to -0.3000, **P = 0.0040. **H**. Confocal images showing the expression of AAV9-NALCN-shRNA-GFP (green) in the VTA DA neurons (DAT, red) (scale bar, 10 μm). **I**. Loose cell-attached current clamp recordings of the spontaneous firing of the male and female VTA DA neurons transfected with either NALCN-shRNA (ii, n = 35, N = 8) or scramble-shRNA (Con, i, n = 30, N = 8) (both GFP and DAT positive). Examples of firing traces in the middle of i and ii and summarized data in the bottom of i were shown. The inset on the top of i and ii shows a map of a coronal midbrain slice indicating the location of GFP^+ neurons that were recorded and subsequently identified as DA neurons which were DAT positive with single cell-PCR (i: Con, grey dots; ii: NALCN-KD, red dots). Mann-Whitney U test, U = 0, ****P < 0.0001. **J**. Whole-cell current clamp recordings

of the resting membrane potential (RMP) of the male VTA DA neurons transfected with either NALCN-shRNA (NALCN-KD, ii, n = 18, N = 5) or scramble-shRNA (Con, i, n = 15, N = 5) (both GFP and DAT positive). Examples of RMP traces in the middle of i and ii and summarized data in the bottom of i were shown. The inset on the top of i and ii shows a map of a coronal midbrain slice indicating the location of GFP^+ neurons that were recorded and subsequently identified as DA neurons which were DAT positive with single cell-PCR (i: Con, grey dots; ii: NALCN-KD, red dots). Mann-Whitney U test, U = 0, ****P < 0.0001. * P < 0.05, ** P < 0.01, **** P < 0.0001. n is number of neurons recorded and N is number of mice used.

Fig. 4 TRP channels contribute to subthreshold depolarization and spontaneous firing of the VTA DA neurons.

A. The expression of TRP channels in VTA DA neurons. i: Single-cell PCR from 5 VTA cells (C1-C5). ii: Percentage of TRP channels (C3, C6 and V2) positive neurons in the VTA DA neurons (DAT positive). **B** and **C**. Example time-course (i), traces (ii) and the summarized data (iii) for the effect of a nonselective cation channel blocker 2-APB (100 μM, n = 12, N = 5 for male mice) (B) and a potent TRPC6 inhibitor LA (10 μM, n = 14, N = 8 for male and female mice) (C) on the spontaneous firing frequency in the VTA DA neurons. The inset on the top of Bii and Cii shows a map of a coronal midbrain slice indicating the location of neurons that were recorded and subsequently identified as DA neurons which were DAT positive with single cell-PCR (red dots). Wilcoxon matched-pairs signed rank test, B: W = -78.00, ***P = 0.0005. C: W = -105.0, ***P = 0.0001. **D** and **E.** Example time-course (i) and the summarized data (ii) for the effect of a nonselective cation channel blocker 2-APB (n = 10, N = 9) (D) and a potent TRPC6 inhibitor LA (n = 9, N = 7) (E) on the resting membrane potential (RMP) of the male and female VTA DA neurons. Paired-sample T test, D: t = 8.082, df = 9, 95% CI: -11.90 to -6.693, ****P < 0.0001, E: t = 6.431, df = 8, 95% CI: -5.993 to -2.829, ***P = 0.0002. *** P < 0.001, **** P < 0.0001.n is number of neurons recorded and N is number of mice used.

Fig. 5 TRPC6 contributes to subthreshold depolarization and spontaneous firing of the VTA DA neurons.

A. The normalized expression profile of TRPC6 in NAc c- and mPFC-projecting VTA

DA neurons was verified using single cell-qPCR (NAc c: n = 28, N = 7; mPFC: n = 25, N=8, both TH positive), Mann-Whitney U test, U = 173, $^{**}P$ = 0.0013. **B**. Confocal images showing co-expression of TRPC6 (green) and TH (red) representing DA neurons (scale bar, 10 μm). **C**. The efficiency of shRNA knockdown of TRPC6 in the VTA verified by qPCR. shRNA against TRPC6 carried by AAV virus (i) (TRPC6-shRNA) was injected into the VTA of mice, the mRNA level in the shRNA-TRPC6 transfected VTA (TRPC6-KD, N = 5) and the scramble shRNA transfected VTA (Con, N = 5) was analyzed using qPCR (ii). Two-sample T test, t = 4.223, df = 8, 95% CI: -0.8194 to -0.2406, $^{**}P$ = 0.0029. **D**. Immunofluorescence labelling showing the expression of AAV9-shRNA(TRPC6)-GFP (green) and DAT (red) in the VTA (scale bar, 10 μm). **E**. Loose cell-attached current clamp recordings of the spontaneous firing of the VTA DA neurons from the mice of both sexes transfected with either TRPC6-shRNA (TRPC6-KD, ii, n = 37, N = 12) or scramble-shRNA (Con, i, n = 27, N = 11) (both GFP and DAT positive). Examples of firing traces in the middle of i and ii and summarized data in the bottom of i were shown. The inset on the top of i and ii shows a map of a coronal midbrain slice indicating the location of GFP^+ neurons that were recorded and subsequently identified as DA neurons which were DAT positive with single cell-PCR (i: Con, grey dots; ii: TRPC6-KD, red dots). Mann-Whitney U test, U = 48, $^{****}P < 0.0001$. **F**. Example time-course (i) and summarized data (ii) showed that shRNA knockdown of TRPC6 in the VTA of male mice decreased the 2-APB-inhibited firing responses of the VTA DA neurons. The inset on the top of ii shows a map of a coronal midbrain slice indicating the location of GFP^+ neurons that were recorded and subsequently identified as DA neurons which were DAT positive with single cell-PCR (TRPC6-KD, red dots). (n = 7, N = 5, both GFP and DAT positive), Wilcoxon matched-pairs signed rank test, W = -18.00, P = 0.1563. **G**. Whole-cell current clamp recordings of the resting membrane potential (RMP) of the male mice VTA DA neurons transfected with either TRPC6-shRNA (TRPC6-KD, ii, n = 10, N = 6) or scramble-shRNA (Con, i, n = 10, N = 6) (both GFP and DAT positive). Examples of RMP traces in the middle of i and ii and summarized data in the bottom of i were shown. The inset on the top of i and ii shows a map of a coronal midbrain slice indicating the location of GFP^+ neurons that were recorded and subsequently identified as DA neurons which were DAT positive with single cell-PCR (i: Con, grey dots; ii: TRPC6-KD, red dots).

Mann-Whitney U test, U = 8, ***P = 0.0007. **H**. Example time-course (i) and summarized data (ii) showed that shRNA knockdown of TRPC6 in the male mice VTA decreased the LA-inhibited firing responses of the VTA DA neurons. The inset on the top of ii shows a map of a coronal midbrain slice indicating the location of GFP^+ neurons that were recorded and subsequently identified as DA neurons which were DAT positive with single cell-PCR (TRPC6-KD, red dots). (n = 8, N = 5, both GFP and DAT positive), Paired-sample T test, t = 0.000, df = 7, 95% CI: -0.05740 to 0.05740, $P > 0.9999$. n.s. $P > 0.05$, ** $P < 0.01$, *** $P < 0.001$, ****$P < 0.0001$. n is number of neurons recorded and N is number of mice used.

Fig. 6 CMUS depression mice have a decreased firing activity and down-regulated TRPC6 expression in the VTA DA neurons.

A. Experimental procedure timeline. **B**. i: Sucrose preference test for CMUS male mice (Con: N = 10; CMUS: N = 10). Two-sample T test, t = 3.569, df = 18, 95% CI: -20.73 to -5.369, **P = 0.0022, compared with control mice. ii: Tail suspension test for CMUS male mice (Con: N = 10; CMUS: N = 10), Two-sample T test, t = 5.826, df = 18, 95% CI: 23.21 to 49.39, ****$P < 0.0001$, compared with control mice. **C**. Loose cell-attached current clamp recordings of the spontaneous firing of the VTA DA neurons from the CMUS (n = 68, N = 33, DAT positive) and the control (n = 53, N = 31, DAT positive) mice of both sexes. The inset on the top of i and ii shows a map of a coronal midbrain slice indicating the location of neurons that were recorded and subsequently identified as DA neurons which were DAT positive with single cell-PCR (i: Con, grey dots; ii: CMUS, red dots). Examples of firing traces in the bottom of i as well as in the bottom left of ii and summarized data in the bottom right of ii were shown. Mann-Whitney U test, U = 415, ****$P < 0.0001$. **D**. Representative Western blot assay (i) and summarized data (ii) showing the expression of TRPC6 and GAPDH in the VTA of the control (Con, N = 10) and the CMUS (N = 11) mice of both sexes. Two-sample T test, t = 5.134, df = 19, 95% CI: -0.7480 to -0.3147, ****$P < 0.0001$. **E**. i and ii: Example traces (up) and time-course (bottom) of firing frequency of mPFC-projecting VTA DA neurons, effect of 2-APB. (i) Con and (ii) CMUS of both sexes. iii. Summarized effect of 2-APB in the control (n = 22 cells, N = 15, DAT positive) and CMUS (n = 25 cells, N = 15, DAT positive) mice. Kruskal-Wallis-H test with Dunnett's multiple comparisons test, Kruskal-Wallis

statistic = 66.03, Con-ACSF *vs*. CMUS-ACSF, $^{**}P$ = 0.0056; Con-2-APB *vs*. CMUS-2-APB, $^{**}P$ = 0.0016; Con-ACSF *vs*. Con-2-APB, $^{****}P < 0.0001$; CMUS-ACSF *vs*. CMUS-2-APB, $P > 0.9999$. iv. The inhibition rate (%) on firing rate by 2-APB in the control group (n = 22, N = 15) and the CMUS group (n = 25, N = 15). Mann-Whitney U test, U = 7, $^{****}P < 0.0001$. The inset on the top of iii and iv shows a map of a coronal midbrain slice indicating the location of mPFC-projecting neurons that were recorded and subsequently identified as DA neurons which were DAT positive with single cell-PCR (iii: Con, grey dots; iv: CMUS, red dots). **F**. i and ii: Example traces (up) and time-course (bottom) of firing frequency of mPFC-projecting VTA DA neurons, effects of LA. (i) Con and (ii) CMUS of both sexes. iii. Summarized effect of LA on the control (n = 25 cells, N = 16, DAT positive) and CMUS (n = 30 cells, N = 18, DAT positive) mice. Kruskal-Wallis-H test with Dunnett's multiple comparisons test, Kruskal-Wallis statistic = 79.59, Con-ACSF *vs*. CMUS-ACSF: $^{****}P < 0.0001$, CON-LA *vs.* CMUS-LA: $^{**}P$ = 0.0026, Con-ACSF *vs*. Con-LA: $^{****}P < 0.0001$, CMUS-ACSF *vs*. CMUS-LA: $P > 0.9999$. iv. The inhibition rate (%) on firing rate by LA in the control group (n = 25, N = 16) and the CMUS group (n = 30, N = 18). Mann-Whitney U test, U = 2, $^{****}P < 0.0001$. The inset on the top of iii and iv shows a map of a coronal midbrain slice indicating the location of mPFC-projecting neurons that were recorded and subsequently identified as DA neurons which were DAT positive with single cell-PCR (iii: Con, grey dots; iv: CMUS, red dots). n.s. $P > 0.05$, $^{**}P < 0.01$, $^{****}P < 0.0001$.n is number of neurons recorded and N is the number of mice used.

Fig. 7 Selective knockdown of TRPC6 in the VTA DA neurons confers the male mice with depression-like and anxiety-like behaviors which are reversed by overexpression of TRPC6.

A. shRNA against TRPC6 carried by AAV-loxp virus (TRPC6-shRNA) was injected into the VTA of the DAT-Cre male mice. **B**. The mRNA level in the shRNA-TRPC6 transfected VTA (TRPC6-cKD) and the scramble shRNA transfected VTA (Con) was analyzed using qPCR (Con: N = 8; TRPC6-cKD: N = 6). Mann-Whitney U test, U = 0, $^{***}P$ = 0.0003. **C**. Immunofluorescence labelling showing the expression of AAV9-hSyn-DIO-shRNA(TRPC6)-RFP (red) and DAT (green) in the VTA of the DAT-Cre mice (scale bar, 10 μm). **D**. The effects of Cre-induced conditional

knockdown of TRPC6 in the VTA DA neurons on the behaviors of mice in the sucrose preference test (i), the tail suspension test (ii), and the elevated plus-maze test (iii, iv) (Con: N = 10; TRPC6-cKD: N = 10). Sucrose preference test: Two-sample T test, t = 4.172, df = 18, 95% CI: -17.07 to -5.634, ***P = 0.0006; Tail suspension test: Two-sample T test, t = 3.377, df = 18, 95% CI: 7.785 to 33.41, **P = 0.0034; Elevated plus-maze test: Mann-Whitney U test, open arm, U = 2, ****P < 0.0001, closed arm, U = 13, **P = 0.0039. **E**. The effects of TRPC6 over-expression in the TRPC6-cKD-induced depression-like behavior. AAV9-DIO-TRPC6-GFP (TRPC6-cOE) was injected into the VTA of the male DAT-Cre mice, 7 days after injection of AAV9-hSyn-DIO-shRNA(TRPC6)-RFP (TRPC6-cKD). **F**. The protein level TRPC6 of VTA (Con: the scramble shRNA for TRPC6, N = 7; C6-cKD: TRPC6-cKD, N = 10; C6-cKD+cOE: TRPC6-cKD+TRPC6-cOE, N = 7). Kruskal-Wallis H test with Dunnett's multiple comparisons test, Kruskal-Wallis statistic = 16.92, Con *vs.* C6-cKD: ***P = 0.0009, C6-cKD *vs.* C6-cKD+cOE: **P = 0.0034. **G**. Immunofluorescence labelling showing the expression of AAV9-hSyn-DIO-shRNA(TRPC6)-RFP (red), AAV9-DIO-TRPC6-GFP (green) and DAT (blue) in the VTA of the DAT-Cre mice (scale bar, 10 μm). **H**. The effects of TRPC6 over-expression on depression-like behaviors of TRPC6-cKD male mice: the sucrose preference test (i), the tail suspension test (ii), and the elevated plus-maze test (iii) (Con: N = 10; C6-cKD: N = 10; C6-cKD+ cOE: N= 10). the sucrose preference test: Kruskal-Wallis H test with Dunnett's multiple comparisons test, Kruskal-Wallis statistic = 12.96, Con *vs.* C6-cKD: **P = 0.0025, C6-cKD *vs.* C6-cKD+cOE: *P = 0.0139; tail suspension test: One-way ANOVA with Dunnett's multiple comparisons test, $F_{(DFn,\ DFd)} = 0.8336_{(2,\ 27)}$, Con *vs.* C6-cKD: **$P$ = 0.0011, C6-cKD *vs.* C6-cKD+cOE: ***P = 0.0003; elevated plus-maze test: One-way ANOVA with Dunnett's multiple comparisons test, $F_{(DFn,\ DFd)} = 4.884_{(2,\ 27)}$, Con *vs.* C6-cKD: ****$P$ < 0.0001, C6-cKD *vs.* C6-cKD+cOE: **P = 0.0023. *P < 0.05, **P < 0.01, ***P < 0.001, ****P < 0.0001.n is number of neurons recorded and N is the number of mice used.

Fig. 8 Selective knockdown of TRPC6 in the mPFC-projecting VTA DA neurons produces depression-like and anxiety-like behaviors.

A. shRNA against TRPC6 carried by retro-AAV-loxp virus (TRPC6-shRNA) was

injected into the mPFC of the DAT-Cre male mice. **B**. The mRNA level in the shRNA-TRPC6 transfected mPFC-projecting VTA (TRPC6-rcKD) DA neurons and the scramble shRNA transfected mPFC-projecting VTA DA neurons (Con) was analyzed using single-cell quantitative PCR (scqPCR)(Con: n = 15, N = 6; TRPC6-rcKD: n = 16, N = 6). Mann-Whitney U test, U =8.500, ****P < 0.0001.**C**. Immunofluorescence labelling showing the expression of AAV-retro-hSyn-DIO-mCherry-shRNA(TRPC6) (red) and DAT (green) in the VTA of the DAT-Cre mice (scale bar, 10 μm). **D**. The effects of Cre-induced conditional knockdown of TRPC6 in mPFC-projecting VTA DA neurons on the behaviors of mice: (i) the sucrose preference test, (ii) the tail suspension test, and (iii) the elevated plus-maze test (Con: N = 10; TRPC6-rcKD: N = 10). Two-sample T test, sucrose preference test: t = 3.592, df = 18, 95% CI: -11.48 to -3.008, **P = 0.0021; tail suspension test: t = 3.707, df = 18, 95% CI: 10.79 to 39.01, **P = 0.0016; elevated plus-maze test: open arm t = 3.756, df = 18, 95% CI: -8.099 to -2.288, **P = 0.0014. **P < 0.01, ****P < 0.0001.n is number of neurons recorded and N is the number of mice used.

Fig. 1

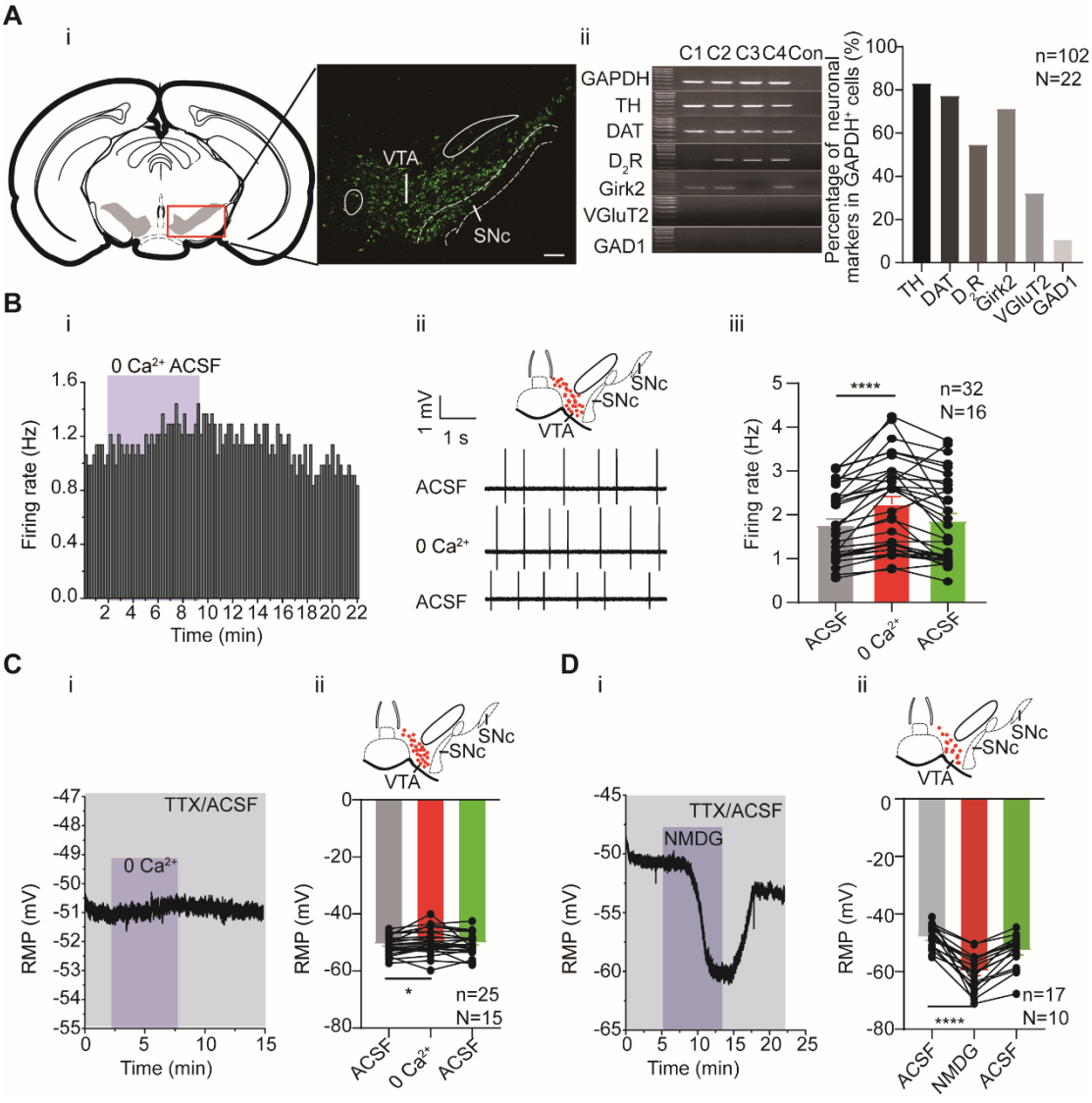
A
i
VTA
SNc
ii
C1 C2 C3 C4 Con
GAPDH
TH
DAT
D2R
Girk2
VGluT2
GAD1
Percentage of neuronal markers in GAPDH+ cells (%)
n=102
N=22
TH
DAT
D2R
Girk2
VGluT2
GAD1
B
i
0 Ca2+ ACSF
Firing rate (Hz)
Time (min)
ii
1 mV
1 s
SNc
VTA
ACSF
0 Ca2+
ACSF
iii
****
n=32
N=16
Firing rate (Hz)
ACSF
0 Ca2+
ACSF
C
i
TTX/ACSF
0 Ca2+
RMP (mV)
Time (min)
ii
SNc
VTA
RMP (mV)
*
n=25
N=15
ACSF
0 Ca2+
ACSF
D
i
TTX/ACSF
NMDG
RMP (mV)
Time (min)
ii
SNc
VTA
RMP (mV)
****
n=17
N=10
ACSF
NMDG
ACSF

1475

Fig. 2

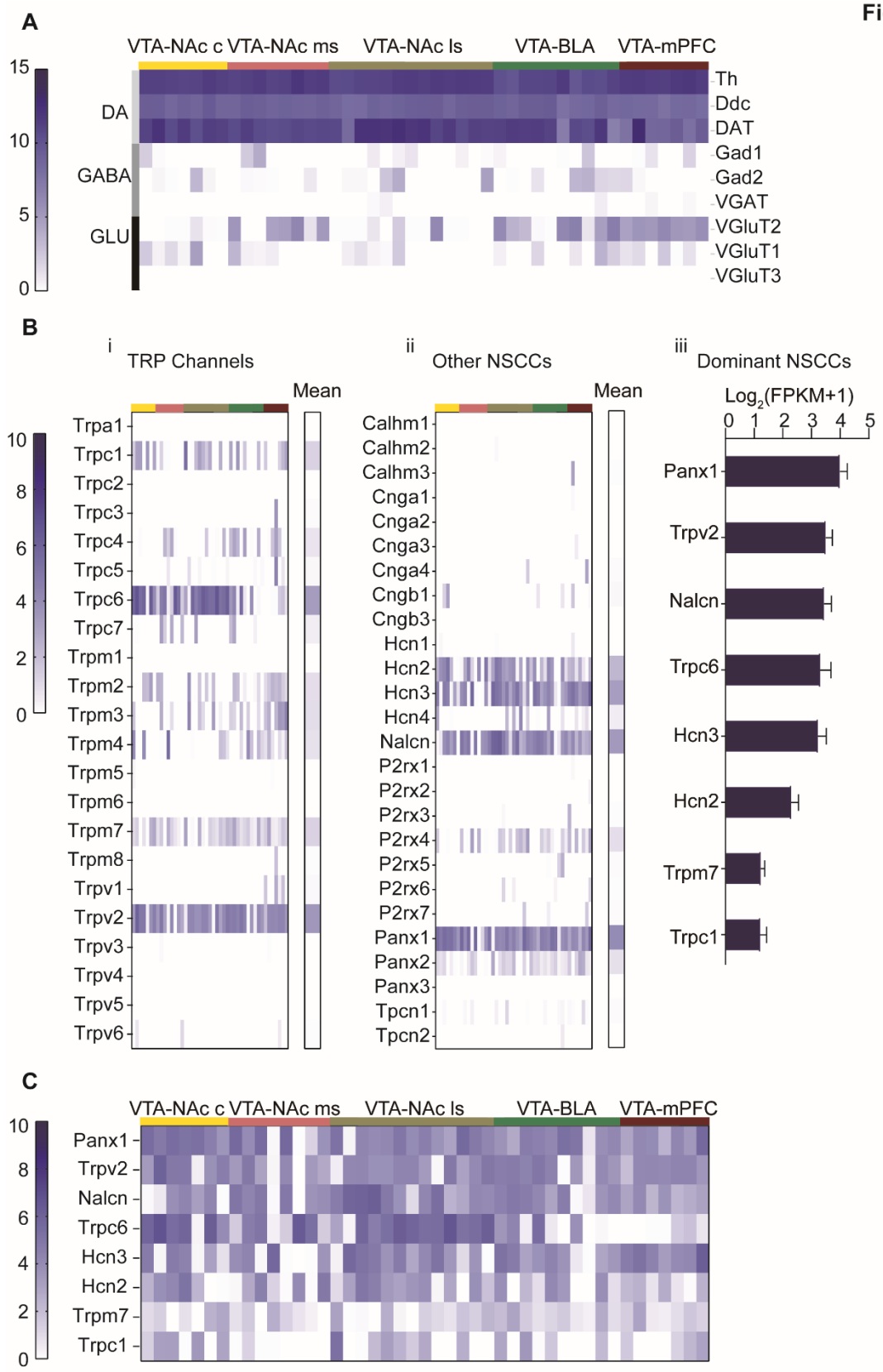
A
VTA-NAc c
VTA-NAc ms
VTA-NAc ls
VTA-BLA
VTA-mPFC
15
10
5
0
DA
GABA
GLU
Th
Ddc
DAT
Gad1
Gad2
VGAT
VGluT2
VGluT1
VGluT3
B
i
TRP Channels
Mean
Trpa1
Trpc1
Trpc2
Trpc3
Trpc4
Trpc5
Trpc6
Trpc7
Trpm1
Trpm2
Trpm3
Trpm4
Trpm5
Trpm6
Trpm7
Trpm8
Trpv1
Trpv2
Trpv3
Trpv4
Trpv5
Trpv6
ii
Other NSCCs
Calhm1
Calhm2
Calhm3
Cnga1
Cnga2
Cnga3
Cnga4
Cngb1
Cngb3
Hcn1
Hcn2
Hcn3
Hcn4
Nalcn
P2rx1
P2rx2
P2rx3
P2rx4
P2rx5
P2rx6
P2rx7
Panx1
Panx2
Panx3
Tpcn1
Tpcn2
iii
Dominant NSCCs
Log2(FPKM+1)
0 1 2 3 4 5
Panx1
Trpv2
Nalcn
Trpc6
Hcn3
Hcn2
Trpm7
Trpc1
C
VTA-NAc c
VTA-NAc ms
VTA-NAc ls
VTA-BLA
VTA-mPFC
Panx1
Trpv2
Nalcn
Trpc6
Hcn3
Hcn2
Trpm7
Trpc1

1476

Fig. 3

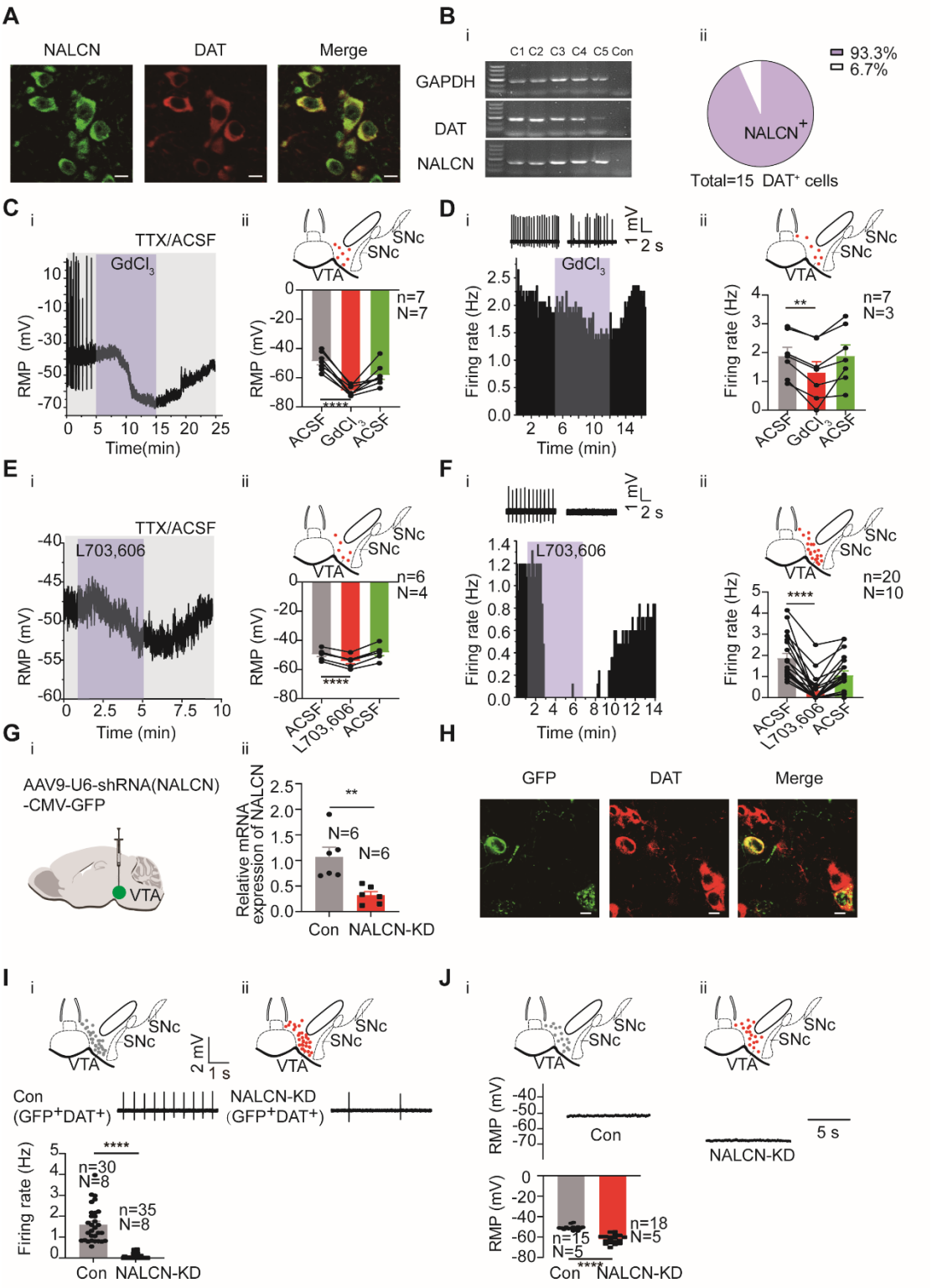
A
NALCN
DAT
Merge
B
i
C1 C2 C3 C4 C5 Con
GAPDH
DAT
NALCN
ii
93.3%
6.7%
NALCN+
Total=15 DAT+ cells
C
i
TTX/ACSF
GdCl3
RMP (mV)
Time(min)
ii
SNc
VTA
n=7
N=7
ACSF
GdCl3
ACSF
D
i
1 mV
2 s
GdCl3
Firing rate (Hz)
Time (min)
ii
n=7
N=3
E
i
TTX/ACSF
L703,606
RMP (mV)
Time (min)
ii
n=6
N=4
ACSF
L703,606
ACSF
F
i
1 mV
2 s
L703,606
Firing rate (Hz)
Time (min)
ii
n=20
N=10
G
i
AAV9-U6-shRNA(NALCN)
-CMV-GFP
VTA
ii
Relative mRNA expression of NALCN
N=6
N=6
Con
NALCN-KD
H
GFP
DAT
Merge
I
i
SNc
VTA
2 mV
1 s
Con
(GFP+DAT+)
ii
NALCN-KD
(GFP+DAT+)
Firing rate (Hz)
n=30
N=8
n=35
N=8
Con
NALCN-KD
J
i
SNc
VTA
RMP (mV)
Con
ii
NALCN-KD
5 s
n=15
N=5
n=18
N=5
Con
NALCN-KD

1477

Fig. 4

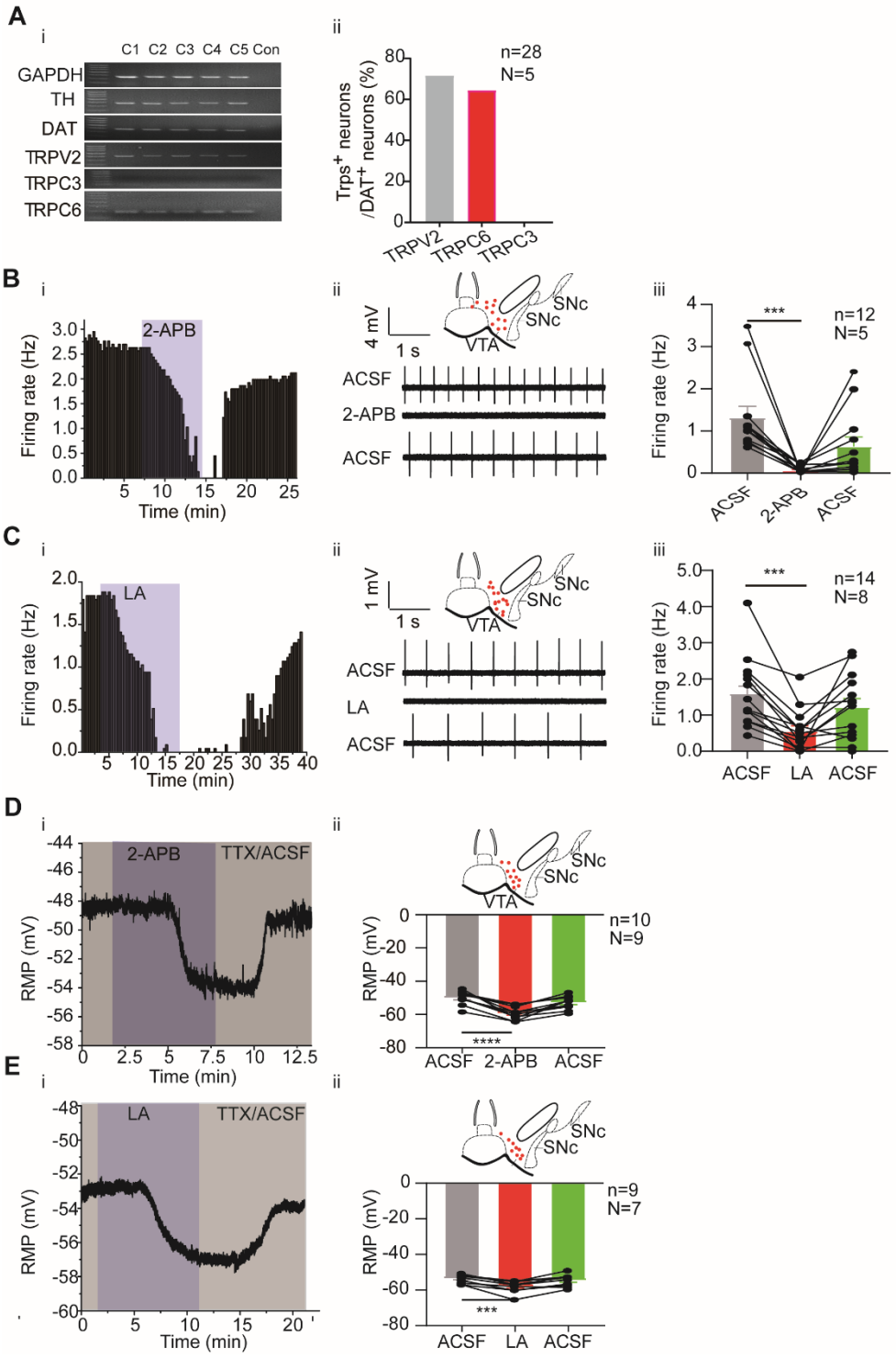
A
i
C1 C2 C3 C4 C5 Con
GAPDH
TH
DAT
TRPV2
TRPC3
TRPC6
ii
Trps+ neurons /DAT+ neurons (%)
n=28
N=5
TRPV2
TRPC6
TRPC3
B
i
2-APB
Firing rate (Hz)
Time (min)
ii
4 mV
1 s
SNc
VTA
ACSF
2-APB
ACSF
iii
***
n=12
N=5
Firing rate (Hz)
ACSF
2-APB
ACSF
C
i
LA
Firing rate (Hz)
Time (min)
ii
1 mV
1 s
SNc
VTA
ACSF
LA
ACSF
iii
***
n=14
N=8
Firing rate (Hz)
ACSF
LA
ACSF
D
i
2-APB
TTX/ACSF
RMP (mV)
Time (min)
ii
SNc
VTA
RMP (mV)
n=10
N=9
****
ACSF
2-APB
ACSF
E
i
LA
TTX/ACSF
RMP (mV)
Time (min)
ii
SNc
RMP (mV)
n=9
N=7
***
ACSF
LA
ACSF

1478

Fig. 5

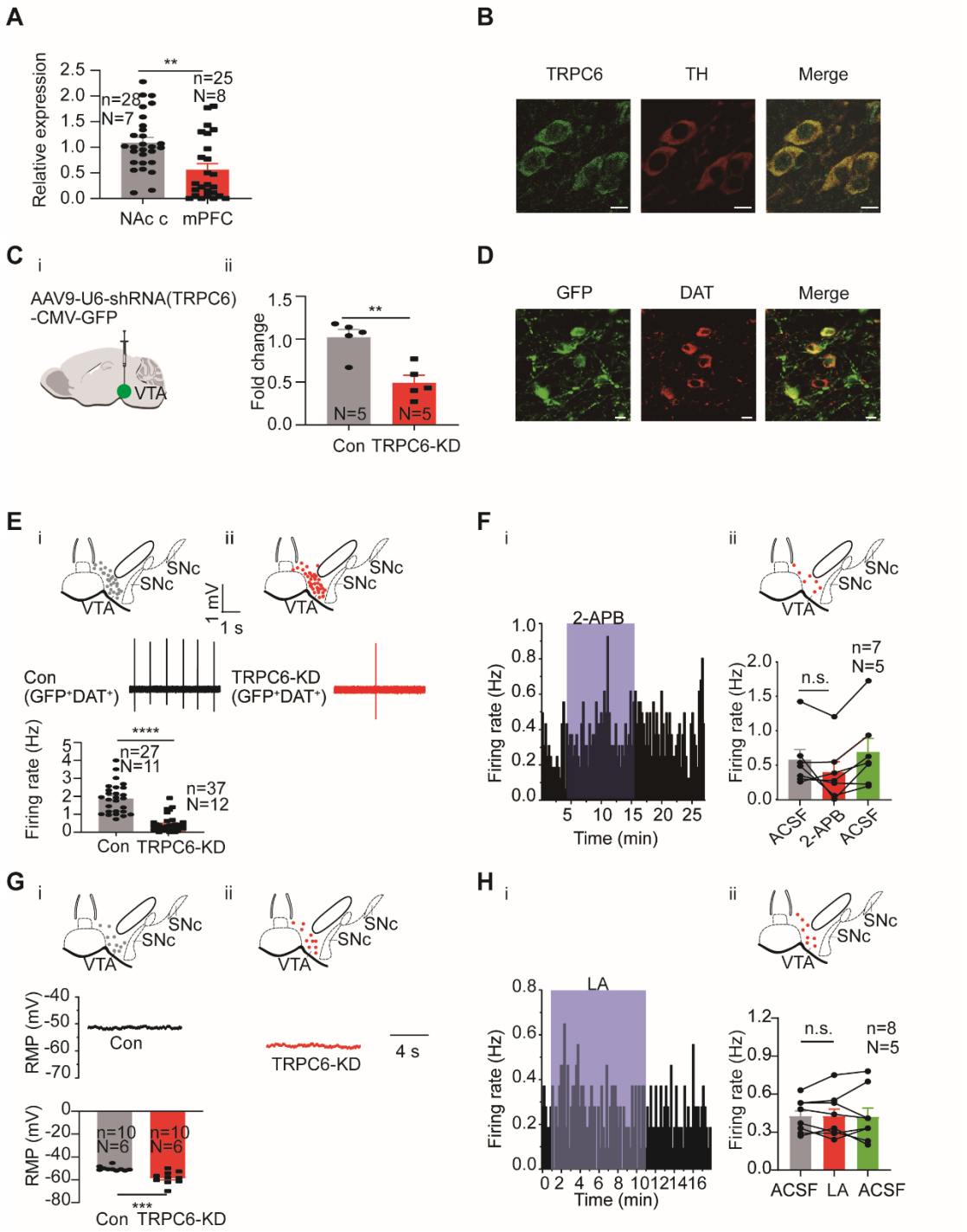
A
Relative expression
2.5
2.0
1.5
1.0
0.5
0.0
**
n=28
N=7
n=25
N=8
NAc c
mPFC
B
TRPC6
TH
Merge
C
i
ii
AAV9-U6-shRNA(TRPC6)
-CMV-GFP
VTA
Fold change
1.5
1.0
0.5
0.0
**
N=5
N=5
Con
TRPC6-KD
D
GFP
DAT
Merge
E
i
ii
SNc
SNc
VTA
1 mV
1 s
Con
(GFP+DAT+)
TRPC6-KD
(GFP+DAT+)
Firing rate (Hz)
****
n=27
N=11
n=37
N=12
Con
TRPC6-KD
F
i
ii
2-APB
Firing rate (Hz)
Time (min)
n.s.
n=7
N=5
ACSF
2-APB
ACSF
G
i
ii
RMP (mV)
Con
TRPC6-KD
4 s
n=10
N=6
n=10
N=6
***
Con
TRPC6-KD
H
i
ii
LA
Firing rate (Hz)
Time (min)
n.s.
n=8
N=5
ACSF
LA
ACSF

1479

Fig. 6

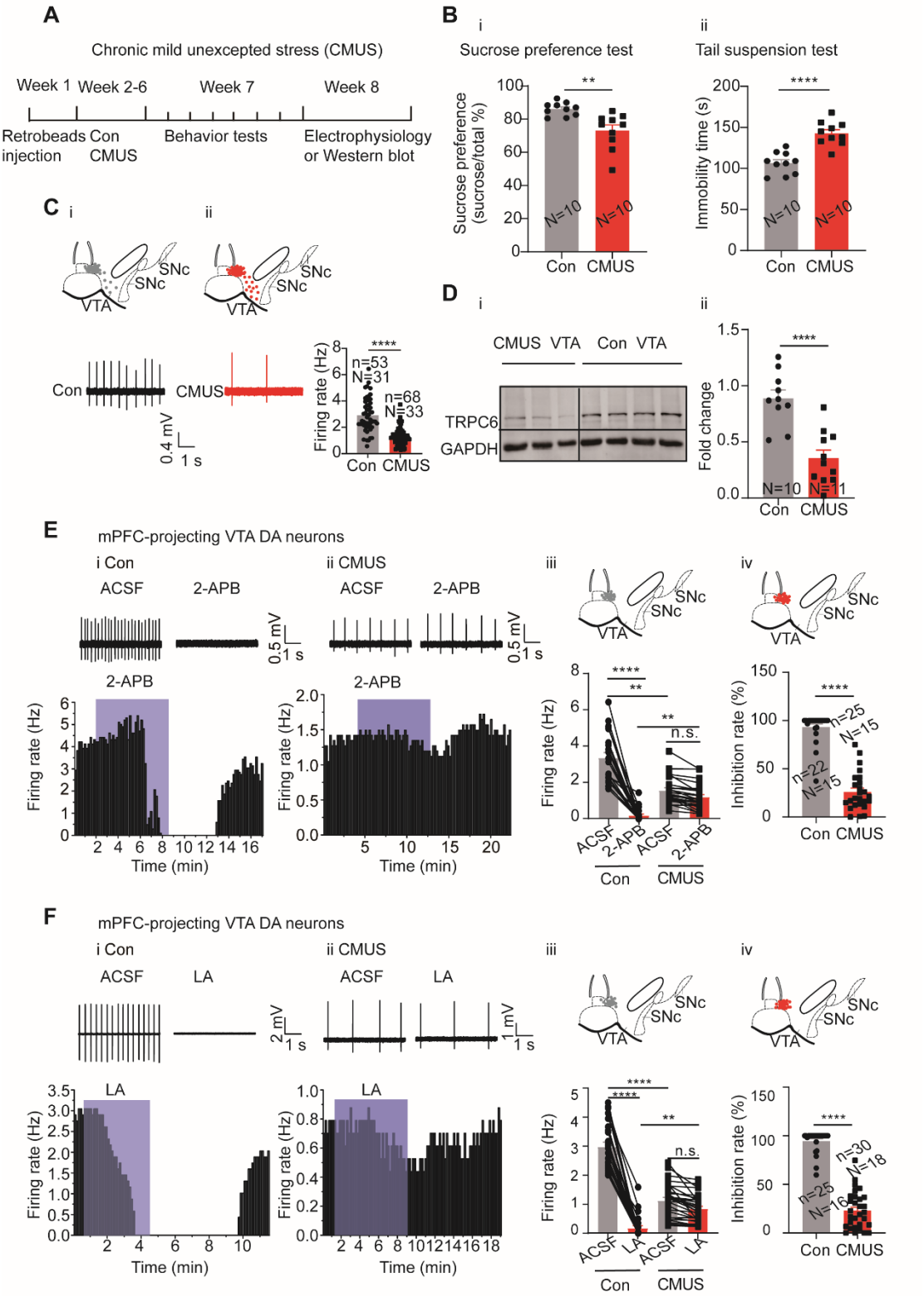
A
Chronic mild unexcepted stress (CMUS)
Week 1
Week 2-6
Week 7
Week 8
Retrobeads injection
Con CMUS
Behavior tests
Electrophysiology or Western blot
B
i
Sucrose preference test
Sucrose preference (sucrose/total %)
N=10
N=10
Con
CMUS
ii
Tail suspension test
Immobility time (s)
N=10
N=10
Con
CMUS
C
i
ii
SNc
VTA
Con
CMUS
0.4 mV
1 s
Firing rate (Hz)
n=53
N=31
n=68
N=33
Con
CMUS
D
i
CMUS VTA
Con VTA
TRPC6
GAPDH
ii
Fold change
N=10
N=11
Con
CMUS
E
mPFC-projecting VTA DA neurons
i Con
ACSF
2-APB
ii CMUS
ACSF
2-APB
0.5 mV
1 s
Firing rate (Hz)
Time (min)
iii
iv
Inhibition rate (%)
n=22
N=15
n=25
N=15
n.s.
Con
CMUS
F
mPFC-projecting VTA DA neurons
i Con
ACSF
LA
ii CMUS
ACSF
LA
2 mV
1 s
1 mV
1 s
Firing rate (Hz)
Time (min)
iii
iv
Inhibition rate (%)
n=25
N=16
n=30
N=18
n.s.
Con
CMUS

1480

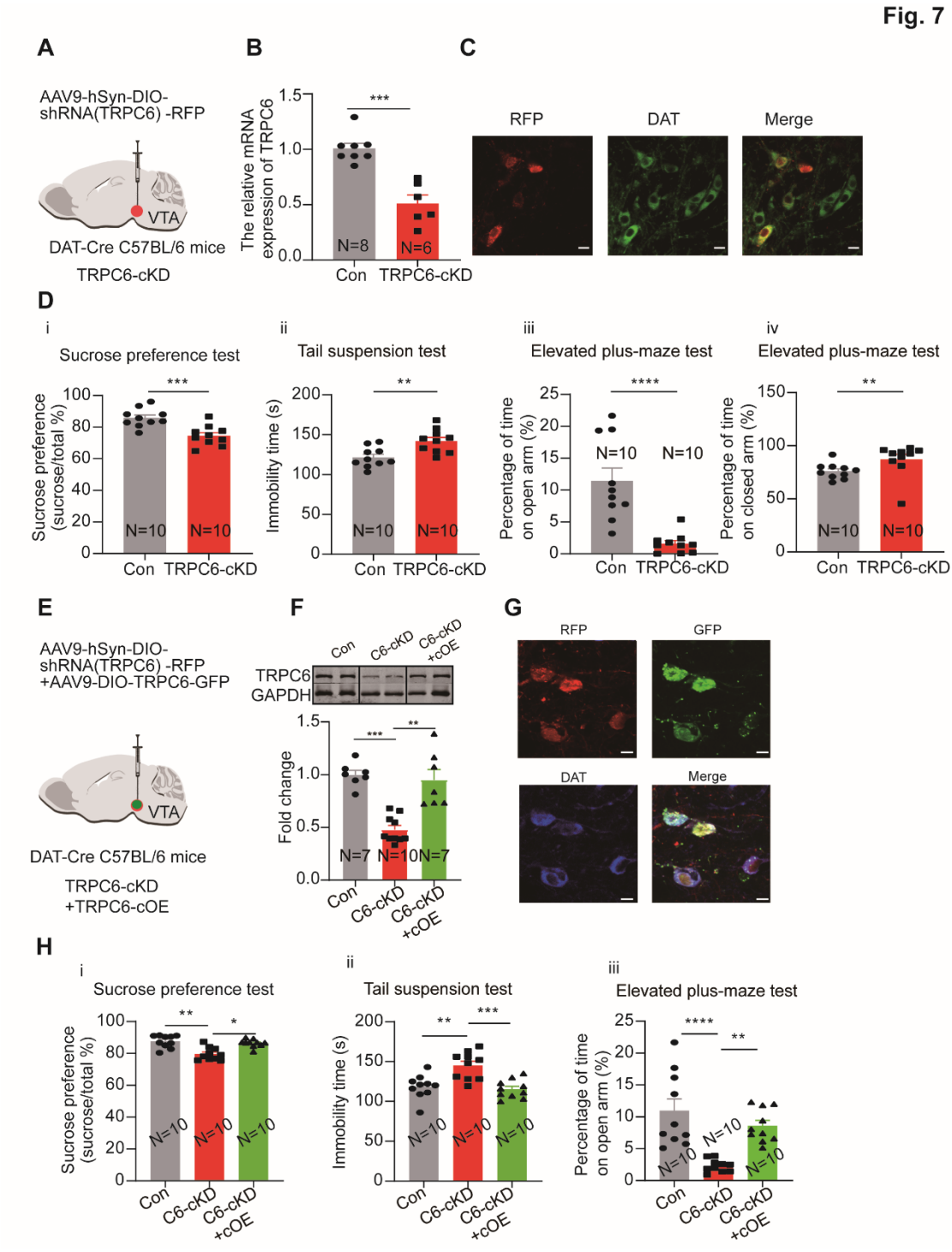
Fig. 7
A
AAV9-hSyn-DIO-shRNA(TRPC6) -RFP
VTA
DAT-Cre C57BL/6 mice
TRPC6-cKD
B
The relative mRNA expression of TRPC6
***
N=8
N=6
Con
TRPC6-cKD
C
RFP
DAT
Merge
D
i
Sucrose preference test
Sucrose preference (sucrose/total %)
***
N=10
N=10
Con
TRPC6-cKD
ii
Tail suspension test
Immobility time (s)
**
N=10
N=10
Con
TRPC6-cKD
iii
Elevated plus-maze test
Percentage of time on open arm (%)
****
N=10
N=10
Con
TRPC6-cKD
iv
Elevated plus-maze test
Percentage of time on closed arm (%)
**
N=10
N=10
Con
TRPC6-cKD
E
AAV9-hSyn-DIO-shRNA(TRPC6) -RFP
+AAV9-DIO-TRPC6-GFP
VTA
DAT-Cre C57BL/6 mice
TRPC6-cKD
+TRPC6-cOE
F
Con
C6-cKD
C6-cKD +cOE
TRPC6
GAPDH
Fold change
***
**
N=7
N=10
N=7
Con
C6-cKD
C6-cKD +cOE
G
RFP
GFP
DAT
Merge
H
i
Sucrose preference test
Sucrose preference (sucrose/total %)
**
*
N=10
N=10
N=10
Con
C6-cKD
C6-cKD +cOE
ii
Tail suspension test
Immobility time (s)
**
***
N=10
N=10
N=10
Con
C6-cKD
C6-cKD +cOE
iii
Elevated plus-maze test
Percentage of time on open arm (%)
****
**
N=10
N=10
N=10
Con
C6-cKD
C6-cKD +cOE

1481

Fig. 8

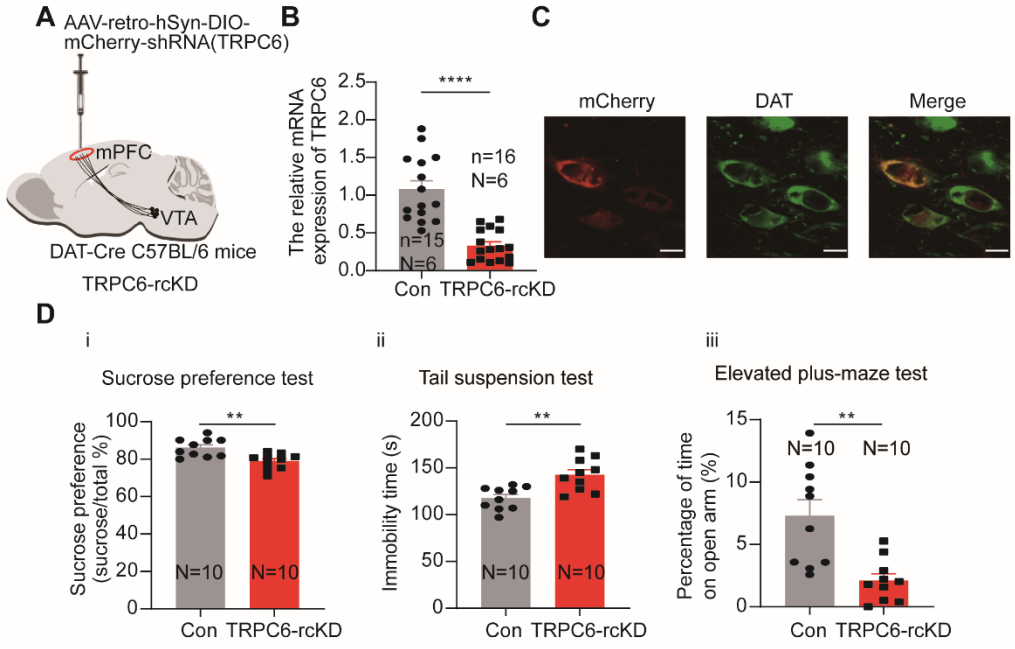
A
AAV-retro-hSyn-DIO-mCherry-shRNA(TRPC6)
mPFC
VTA
DAT-Cre C57BL/6 mice
TRPC6-rcKD
B
The relative mRNA expression of TRPC6
****
n=16
N=6
n=15
N=6
Con
TRPC6-rcKD
C
mCherry
DAT
Merge
D
i
Sucrose preference test
Sucrose preference (sucrose/total %)
**
N=10
N=10
Con
TRPC6-rcKD
ii
Tail suspension test
Immobility time (s)
**
N=10
N=10
Con
TRPC6-rcKD
iii
Elevated plus-maze test
Percentage of time on open arm (%)
**
N=10
N=10
Con
TRPC6-rcKD

1482